Review Article

At-Tasneem Mohd Amin*, Wan Azmi Wan Hamzah, and Ahmed Nurye Oumer

Thermal conductivity and dynamic viscosity of mono and hybrid organic- and synthetic-based nanofluids: A critical review

https://doi.org/10.1515/ntrev-2021-0086
received July 14, 2021; accepted August 27, 2021

Abstract: Thermal conductivity and dynamic viscosity are two critical properties of nanofluids that indicate their heat transfer performance and flow. Nanofluids are prepared by dispersing mono or several organic or synthetic nanoparticles in selected base fluids to form mono or hybrid nanofluids. The qualitative and quantitative stability measurement of nanofluids will then be addressed, followed by a detailed discussion on how the dispersion of nanoparticles in water (W), ethylene glycol (EG), and the mixture of W:EG 60:40% by volume affects the thermal conductivity and dynamic viscosity ratio. The data comparison demonstrated that the thermal conductivity ratio increases with increasing normalized concentrations, the bulk temperature of nanofluids, and the smaller nanoparticle size. The dynamic viscosity ratio is multiplied by the normalized concentration increase. Nevertheless, as the bulk temperature climbed from 0 to 80°C, the dynamic viscosity ratio was scattered, and the dynamic viscosity ratio trend dropped with increasing particle size. While the majority of nanofluids enhanced thermal conductivity ratio by 20%, adding carbon-based nanoparticles to synthetic nanofluid increased it by less than 10%. The disadvantage of nanofluids is that they multiply the dynamic viscosity ratio of all nanofluids, which increase power consumption and reduces the efficiency of any mechanical system.

Keywords: hybrid nanofluids, thermal conductivity, dynamic viscosity

*** Corresponding author: At-Tasneem Mohd Amin,** Faculty of Mechanical and Automotive Engineering Technology, Universiti Malaysia Pahang, 26600 Pekan, Pahang, Malaysia, e-mail: tasneem@ump.edu.my, tel: +60-9424-6211
Wan Azmi Wan Hamzah, Ahmed Nurye Oumer: Department of Mechanical Engineering, College of Engineering, Universiti Malaysia Pahang, 26300 Gambang, Pahang, Malaysia

Abbreviations

W	water
EG	ethylene glycol
PG	propylene glycol
Ag	silver
Au	gold
Cu	copper
Al	aluminum
Al_2O_3	aluminum oxide
CuO	copper oxide
TiO_2	titanium oxide
ZnO	zinc oxide
SiO	silicon oxide
SiO_2	silicon dioxide
CNT	carbon nanotube
MWCNT	multi-walled carbon nanotubes
GE	graphene
GNP	graphene nanoplatelet
GO	graphene oxide
rGO	reduced graphene oxide
FLG	few layers graphene
FGO	flourinated graphene oxide
GQD	graphene quantum dots
VEM	vacuum evaporation method
EEW	electrical explosion of wire
SANSS	submerged arc nanoparticles synthesis systems
VERL	vacuum evaporation process for running liquids
SEM	scanning electron microscopy
TEM	transmission electron microscopy
FESEM	field emission scanning electron microscopy
IEP	isoelectric point
φ	volume concentration
φ_1	volume concentration of nanofluid at higher concentration
φ_2	volume concentration of nanofluid at lower concentration

ω	weight concentration of nanofluid
wt%	weight percent
vol%	volume percent
ρ_{bf}	density of the base fluid
ρ_{np}	density of nanoparticle
V_1	volume of nanofluid at higher concentration
V_2	volume of nanofluid at lower concentration
C_N	normalized weight or volume concentration
k_r	thermal conductivity ratio
μ_r	dynamic viscosity ratio

1 Introduction

Researchers shifted their focus from a behavioral study of solid milli- and micro-sized particle dispersion in the base fluid to nano-sized particles over a decade ago because nano-sized particles can generate cost-effective and efficient economic growth [1]. A nanoparticle is a solid nano-sized material with a size ranging from 0.1 to 100 nm [2]. Nanofibers, nanotubes, nanowires, nanorods, nanosheet, or droplets have the same definition. Nanoparticles have a high surface area density and heat capacity in the base fluid, remaining in suspension almost indefinitely [3,4]. At the same time, the collision of nanoparticles through the randomness of fluid during the nanofluid mixing process provides a strong interaction between and around nanoparticles. This interaction has a strong potential to improve the thermal conductivity of nanofluids composed of a lower thermal conductivity of base fluid combined with a higher order of magnitude of thermal conductivity of well-dispersed nanoparticle suspension. Yoo *et al.* [5] reported that, in addition to other factors, the surface-to-volume ratio and thermal conductivity of nanoparticles are two critical factors in determining the thermal conductivity of nanofluids. Therefore, nanofluids are widely used to boost mechanical cooling systems, including engine, nuclear reactors, buildings and electronics, and various kinds of heat sources [6–8]. Synthetic-based nanofluids used in a wide range of engineering applications, including solar energy [9–11], heat exchanger, radiator and engine cooling [12–14], and improve the efficiency of the machining process [15–17]. Simultaneously, nanofluids alter the dynamic viscosity of the base fluid, which offers a wide range of advantages for the rheological performance of the flow, including drag reduction of oil pipelines, oil well operation, floodwater drainage, firefighting, field irrigation, transport of suspensions and slurries, sewer systems, water heating and cooling systems, aeronautical tank filling, marine systems, and biomedical systems including blood flow [18–21].

Numerous review papers discuss the effect of different types of nanoparticles dispersed in a base fluid on nanofluids' thermal conductivity and dynamic viscosity. Murshed and Estellé [22] conducted a survey of the number of published review papers on the Internet on the thermophysical characteristics of nanofluids from 2006 to 2015. The authors discovered that most reported reviews on nanofluids are for thermal conductivity (56%), followed by dynamic viscosity (24%). These data demonstrate that nanofluids were mainly lauded for its thermal properties rather than its rheological properties. While the contribution of nanoparticles to increasing the thermal conductivity of the base fluid should be celebrated and recognized, the presence of these substances that affect the rheological properties of the base fluid should not be overlooked because this parameter also contributes to system efficiency. As a result, Al Shdaifat *et al.* [23] investigated the effects of nanoparticle concentration, material, and size on both the thermal and hydraulic performance of water-based CuO nanofluids. Eshgarf *et al.* [24] studied the synthesis, stability, and thermo-physical properties of hybrid nanofluids designed to maximize energy consumption. Zainon and Azmi [25] provided a thorough assessment of the type of nanoparticles, particle volume concentration, particle size and shape, temperature, and base fluid influences on the thermo-hydraulic properties of nanofluids. Pavia *et al.* [26] explored how a minimum amount of graphene (GE) should be dispersed in a base fluid to improve thermal performance with minimal dynamic viscosity to optimize energy usage.

Like the publications before it, this study examined both the thermal conductivity and dynamic viscosity of nanofluids. Nevertheless, the performance of each nanofluid is evaluated by comparing the effect on both parameters of nanofluids due to various factors. The comparison was carried out by using the normalized concentrations of the studied nanofluids and a few other factors that influence these parameters. Section 2 introduces the many types of synthetic- and organic-based nanoparticles that are often used in the literature. The preparation of nanofluids in one or two steps will be explored in Section 3. Sections 4 and 5 will go into the various morphological observations and stability methods for examining the nanofluids' characteristics. Finally, in Section 6, the numerous factors that influence the increase in thermal conductivity and dynamic viscosity will be thoroughly explored, followed by a brief author observation in Section 7.

2 Synthetic- and organic-based nanoparticles

Before selecting the appropriate types of nanoparticles to be dispersed in a base fluid, researchers must consider various factors, including the thermophysical properties of the raw material, the compatibility of the material with the desired base fluid and its safety [27]. Depending on the purpose of the research and where nanofluids are used, nanoparticles used to prepare nanofluids may be divided into two main categories, namely synthetic and organic nanoparticles.

2.1 Synthetic-based nanoparticles

Synthetic nanoparticles can be classified as metallic or non-metallic nanoparticles. Metals such as silver (Ag), gold (Au), copper (Cu), aluminum, and metal oxide or ceramic nanoparticles such as aluminum oxide (Al_2O_3), copper oxide (CuO), titanium oxide (TiO_2), zinc oxide (ZnO), and silicon oxide (SiO) are among the preferred metallic materials used in nanofluid investigations. Metal oxides are commonly used in nanofluids because they are oxidizing resistant and chemically stable [27,28]. In addition, they have a relatively lower density compared to their respective metals. As a result, the metal oxides have a slower settling process, which can improve stability during nanofluid preparation. Nevertheless, Eastman *et al.* [29] stated that pure metal nanoparticles have greater dispersal and thermal conductivity than metal oxide nanoparticles in the base fluid.

Non-metallic nanoparticles are mostly made from carbon-based materials. Carbon-based nanoparticles have attracted the attention of nanofluid researchers due to their superior thermal, electrochemical, and mechanical properties, as well as their excellent corrosion resistance and high aspect ratio (AR). Fullerenes, single and multi-walled carbon nanotubes (MWCNT), GE, and nanodiamonds are zero-, one-, two-, and three-dimensional carbon sheets, respectively [30]. This unique structure has attracted a lot of attention because it takes full advantage of its surface–to–volume ratio and excellent thermal conductivity, a critical characteristic for drag reduction and heat transfer enhancement [31]. GE, in particular, has several varieties based on its functionalization and characteristics. Graphene nanoplatelets (GNP), graphene flakes, graphene oxide (GO), reduced graphene oxide (rGO), fluorinated graphene oxide (FGO), few layers graphene (FLG), graphene quantum dots (GQD), nitrogen-doped GE, and highly fluorinated GO are only a few examples. Jiang *et al.* [32] and Pavia *et al.* [26] discuss the characteristics of each GE and its thermal conductivity. The covenant functionalization process was carried out to reduce aggregation between carbon nanoparticles, which ultimately improves the thermal characteristics of GE and its stability in the base fluid [33].

A recent publication by Hamze *et al.* [34] published a study on the thermal conductivity performance of FLG. FLG was synthesized in the lab from commercial expanded GE using a mechanical exfoliation method aided by tannic acid and dissolved in deionized water. The FLG was dispersed in Tyfocor, a commercial water–propylene glycol-based fluid with a 40:60% ratio of the two. The FLG nanoparticles were characterized using scanning electron microscopy (SEM) and transmission electron microscopy (TEM), which revealed very thin three to five sheet layers with a thickness of 1–2 nm, proving that the FLG nanoparticles were generated. The thermal conductivity of the FLG-Tyfocor was improved by up to 25% at a weight concentration of 0.5 wt% using Triton X-100 surfactants, which had a 1% effect on thermal conductivity. For the same base fluid and concentration, FLG-dynamic Tyfocor's viscosity rose by up to 34.5% [35]. MWCNT, on the other hand, are frequently chosen by mixing them with metal or metal oxide to improve heat transfer and water drag reduction. Nanodiamonds require prior treatment to achieve their characteristics. Sundar *et al.* [36] used sulfuric acid coupled with nitric acid to disperse a large amount of amorphous carbon impurities containing ultra-dispersed diamonds, followed by 72 h of magnetic stirring to make nanodiamonds. Unfortunately, carbon-based nanoparticles have several drawbacks, including equipment depreciation, high costs, and environmentally unfavorable ingredients [37].

2.2 Organic-based nanoparticles

Although synthetic-based nanofluids are well known for their ability to improve thermal-hydraulic performance, a few studies have proposed organic-based nanoparticles as an alternative to synthetic-based nanofluids. It was made using various natural materials, including wood, plants, soil, and others, to have a low environmental impact because it is recyclable and biodegradable. Organic-based nanofluids are also believed to be less harmful to humans, animals, and aquatic organisms [38].

Farhanian *et al.* [39] discovered that urban solid waste has the potential for thermal conductivity, electrical conductivity, and thermal stability in any nanofluid

application. The fly ash was functionalized using a technique known as photo-initiated chemical vapor deposition to create low-cost, low-grade nanoparticles. It was then dispersed in water to separate the lighter and heavier particles. The lighter particles that remain in the supernatant liquid are analyzed to determine the synthesis of nanoparticles. The electrical discharge machining spectrum of fly ash nanoparticles features a few nanofillers, such as CuO, iron oxide, ZnO, and Al_2O_3, which have been proven to improve the thermal performance of nanofluids. Awua *et al.* [40] and Sharifpur *et al.* [38] investigated the possibility of lab synthesized nanoparticles extracted from palm kernel fiber and mango bark, respectively, as a replacement for synthetic nanofluids in any thermal system. The sample was dried, ball-milled, and subjected to SEM and TEM characterization tests. The particle size average for both samples was measured to be 100 nm. The palm kernel fiber was mixed into a W:EG mixture in the percentages of 50:50 and 60:40. Thermal conductivity was enhanced by 16 and 18% for W:EG 50:50 and 60:40, respectively. Nonetheless, the results reveal that there is no significant increase in thermal conductivity for water-based mango bark.

Recent research has demonstrated that when hybrid organic-based nanoparticles are mixed with specific synthetic-based nanoparticles, they provide exceptional thermal performance for nanofluids. Shirazi *et al.* [41] studied the thermo-electrical properties of empty fruit bunch (EFB) pulp, which is classified as food waste. A hybrid of EFB and GO was produced in a one-step method and then thermally treated at 800°C. The findings demonstrated that EFB pulp potentially increased the thermal conductivity of an EG-based fluid by 10.16% at 35°C with a weight concentration of 0.06%. Electrical conductivity also improved significantly by 11,433%. Sadri *et al.* [37] produced a heat transfer system nanocoolant composed of hybrid clove-graphene nanoplatelet (CGNP). The GNP was functionalized with clove buds in a one-pot technique and characterized using X-ray photoelectron, TEM, and stability testing. At 45°C, the thermal conductivity of CGNP rose by 22.92% at a weight concentration of 0.1%. Simultaneously, low-concentration CGNP was utilized to prevent a significant increase in the dynamic viscosity of water-based CGNP.

Dynamic viscosity is an important characteristic that influences pumping power and pressure. Low dynamic viscosity is preferred in heat transfer, and a substantial dynamic viscosity value may be required for any lubrication application. Adewumi *et al.* [42] examined the dynamic viscosity of W:EG-based carbon fiber. The carbon fiber was self-synthesized in the laboratory and had an average diameter of 30–60 nm. Carbon fiber dispersion's dynamic viscosity is stable with temperature but increases dramatically with mass fraction. Gharehkhani *et al.* [43] studied the rheological properties of nanocrystalline cellulose (NCC) synthesized from Acacia mangium fiber hybridized with kenaf fiber pulp. The kenaf fiber was mechanically processed, and the NCC suspension was chemically processed before being mixed for analysis. The results demonstrate that, compared to water-based kenaf, the hybrid water-based kenaf/NCC had a lower viscosity. The limited amount of rigid rod-like particles of NCC with a negative charge act as a rigid particle, preventing the fiber from entangling and bending to create floccettes and flocs, which contribute to the fluid's high viscosity.

Figure 1(a and b) shows the thermal conductivity of selected synthetic and organic nanomaterials as well as a few commonly used nanoparticles. The statistics show schematically that synthetic-based nanoparticles have a higher thermal conductivity than organic-based nanoparticles. Many organic-based nanoparticles such as rice husk, clay, sugar cane fiber, and wood pulp have lower thermal conductivity than the base fluid. While synthetic-based nanoparticles have superior thermal and mechanical properties than organic-based nanoparticles, they have very minimal biodegradable properties that concern environmental and economic impacts [44]. Therefore, in addition to investigating the effectiveness of organic-based nanoparticles for thermal and rheological performance, organic-based nanoparticles have been studied

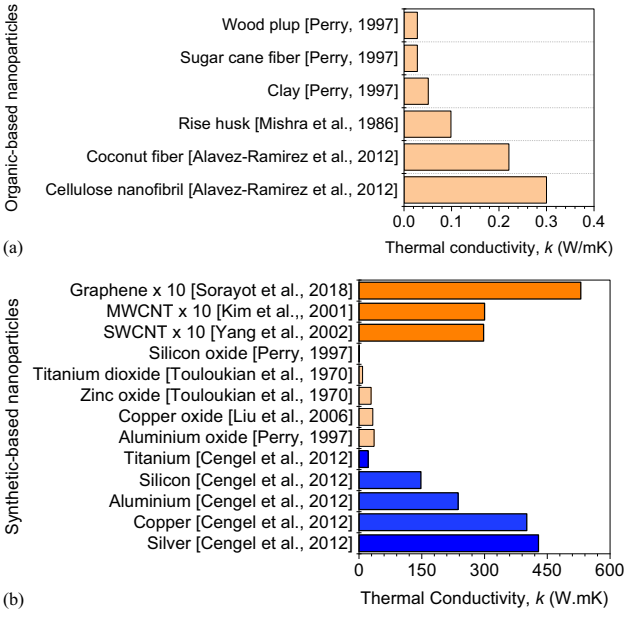

Figure 1: Thermal conductivity of various types of nanoparticles: (a) organic-based nanoparticles and (b) synthetic-based nanoparticles.

for other applications. Nano-additives derived from rice husk are used in biodiesel to reduce emissions and improve direct injection ignition compression engine efficiency [45,46]. The nanoscale of tridax procumbens leaf nanoparticles and aloe vera were used to control bacterial infection in the fabric and as a UV block to preserve the textile color [47,48].

3 Nanofluids preparation

Synthesis of synthetic- and organic-based nanoparticles is crucial for nanofluids. It directly affects nanofluid stability and its thermophysical properties such as thermal conductivity, viscosity, latent heats, surface tension, specific heat capacity, and supercooling [49]. Nanoparticles can be synthesized using two methods: the top-down and bottom-up methods [50–52]. The top-down approach is used when the nanoparticles are synthesized from bulk materials. The size is gradually reduced by various mechanical, chemical, or physical methods until nano-sized particles have been achieved. On the other hand, bottom-up methods involve joining or merging molecules, atoms, or particles smaller than nano-sized particles into a nanoparticle. Then, nanofluid can be prepared by dispersing nanoparticles in a base fluid using one-step or two-step methods.

3.1 One-step method

The one-step method combined the production and dispersion of nanofluids in a single step. This method is helpful as it prevents the oxidation of nanoparticles [53]. At the same time, this method prevents the tiring stage of the drying, sorting, and dispersion of nanoparticles [54]. Various methods of the one-step method have been proposed in the literature. Methods can be classified as physical and chemical processes. The vacuum evaporation method, electrical explosion of wire (EEW), and submerged arc nanoparticles synthesis systems (SANSS) are just a few examples of a one-step method in a physical process.

Vacuum evaporation method is a method of synthesizing nanoparticles in a non-aqueous, low vapor pressure liquid, such as oil and resin. The ultrafine particles of ferromagnetic metals (Fe, Co, and Ni) are evaporated on the surface of the running oil layer, enclosed in a vacuum, flowing out of the spinning disk after continuous application of centrifugal force. Ultra-fine metals were collected in an oil container and formed on the oil surface. The vacuum evaporation method was then adjusted as vacuum evaporation process for running liquids (VERL) or a sputtering method. This method is used for high-pressure magnetron sputtering (up to 50 Pa) of Ag and Fe with low argon sputtering atmospheric. The rotating stainless steel drum consists of layers of a material that rotate between 0 and 19 rpm in a liquid reservoir, such as pumping oil, resins, precursor polymers [55], mineral oil, and silicone oil [56]. The chamber was filled with vacuum air and then flooded with argon to the desired pressure level (1–30 Pa). The sputtering goal and liquid reservoir were then water-cooled. This method produced 5–18 nm of nanoparticles, and the size increased as the pressure range increased [55,56]. The advantages of VERL are as follows [55]:

1) nanoparticles with high melting point material can be synthesized,
2) evaporation condition can be performed in a safe condition,
3) the heat load of the liquid substance is reduced.

On the other hand, EEW was formed in a liquid process containing a mixture of deionized water, oil, glycerine, alcohol, acetone, EG, and hydrogen peroxide by placing the electrodes. This method can produce a wide range of materials that could be shaped into thin wires, with the same material being formed into nanoparticles. The surfactant may be added to the liquid to preserve the stability of synthesized nanoparticles. The key benefit of this method is that it is the most economical to manufacture nanoparticles on a large scale [57].

SANSS were used to synthesize CuO nanofluids [58]. The pure Cu rod was immersed in deionized water in the vacuum chamber, melted, and evaporated by submerged arcs at very high temperatures between 6,000 and 12,000°C. The vaporized metal underwent three phases of the metal vaporization cycle, which for the nanoparticles to be formed are nucleation, growth, and condensation at high vapor pressure and low deionized water temperature. The submerged synthesized nanoparticles then underwent scale analysis before being deposited in a collector. Chang and Chang used the same method for synthesizing Al_2O_3 using a plasma arc as heating element [59]. Other methods proposed in the literature include hydrothermal [60,61], single beam [62], and multi-beam laser ablation [63].

On the other hand, the chemical approach has a significant advantage in synthesizing nanoparticles, which is quicker and cheaper than physical methods [64]. The

sol–gel process is used to synthesize metal oxide or monomers through a bottom-up nanoparticle production method. Small molecules of a colloidal solution (sol) that serve as a precursor become an interconnected (gel) network of discrete particles or polymers [65]. The synthesis process involved the mechanical mixing of extremely small metal oxide (1–2 nm) in water for the 3D inorganic oxide network. The sol then undergoes a casting process to shape and freeze, allowing 3D networks to bind and agglomerate. Through this process, the properties of nanoparticles are determined. Subsequently, the aging process or syneresis is performed to increase the thickness of interparticle necks and reduce the porosity prior to the drying and densification of the pores in gel and to set the density of the metal oxide. Aghababazadeh *et al.* [66] used a modified sol–gel process with an environmentally low-cost binder to synthesize nanocrystalline alumina powder in the range of 15–30 nm. Mishra *et al.* [67] synthesized uniform ZnO spherical particles using the sol–gel process at various annealing temperatures between 500 and 600°C.

One downside of the one-step method is that it is not feasible for mass production, as some of the techniques required a vacuum to slow down the production process and high costs [68]. Physical methods were more preferable for the production of nanoparticles compared to the chemical method since they produce sizes below 100 nm, have a narrow size distribution, and the nanoparticles are isolated from one another [58,69].

3.2 Two-step method

The two-step method is widely used in the preparation of nanofluids as it is more economically efficient. It involves two separate phases: nanoparticles' production by a chemical, physical, or mechanical process and nanoparticles' dispersion to a stable solution. Barki *et al.* [70], Sharifpur *et al.* [38], Panithasan *et al.* [45], and Vinukumar *et al.* [46] used top-down methods to synthesize organic-based nanoparticles such as mango bark and rice husk nanoparticles before using a two-step method to prepare nanofluids. The raw material was washed, cut into small pieces, dried for a long time at a constant temperature, ground or ball milled for a certain period, and sifted until the size of the particles was reduced to that of nano-sized particles. The organic-based nanoparticles were then dispersed in the base fluid and stirred to a homogeneous state. Esmaeili *et al.* [71] used a non-expensive process of mechanochemical ball milling to ground a non-toxic ceramic known as aluminum nitride-carbon nanocomposite for a heat transfer experiment. The nanoparticles were then dispersed in EG without the use of any surfactant. Besides that, the preparation of nanofluids using commercially obtained synthetic nanoparticles such as Au, Ag, Cu, Al_2O_3, CuO, SiO, titanium dioxide, ZnO, aluminum nitride, and GO can be referred to in Haddad *et al.* [72], Devendiran and Amirtham [8], Mahbubul [64], Jamkhande *et al.* [52], Asadi *et al.* [73], and Arshad *et al.* [74].

The range of mass or volume concentration of nanoparticles in a base fluid shall be determined based on the desired research purposes. equations (1) and (2) are used to calculate the weight concentration, ω and volume concentration, ϕ [75], respectively.

$$\omega = \frac{m_{\mathrm{np}}}{m_{\mathrm{np}} + m_{\mathrm{bf}}} \times 100 \tag{1}$$

$$\phi = \frac{m_{\mathrm{np}}/\rho_{\mathrm{np}}}{m_{\mathrm{np}}/\rho_{\mathrm{np}} + m_{\mathrm{bf}}/\rho_{\mathrm{bf}}} \times 100 \tag{2}$$

Nanofluids can be prepared using one type of nanoparticle or a mixture of more than one type of nanoparticle dispersed in the base fluid and generally referred to as mono- and hybrid nanofluids. Hybrid nanofluid is a new generation of nanofluids. It incorporated two or more different types of nanoparticles to optimize the use of positive characteristics and reduce the limitation of each nanoparticle. The idea of mixing two or more nanoparticles in a base fluid is to further amplify the thermophysical properties and pressure drop characteristics through a trade-off between the advantages and disadvantages of individual suspensions due to the excellent AR, stronger thermal networks, and the synergistic effect of nanomaterials [76]. The challenges, however, are the choice and the preparation of appropriate hybrid nanoparticles, the stability of the hybrid nanofluid, and limited thermal conductivity models of hybrid nanofluids [77]. The volume concentration, φ of hybrid nanofluid is calculated as [75]

$$\varphi = \frac{\omega\rho_{\mathrm{bf}}}{\left(1 - \frac{\omega}{100}\right)\rho_{\mathrm{np}} + \frac{\omega}{100}\rho_{\mathrm{bf}}} \tag{3}$$

$$\Delta V = (V_2 - V_1) = V_1\left(\frac{\varphi_1}{\varphi_2} - 1\right) \tag{4}$$

where ω, ρ_{bf}, ρ_{np}, V_2, and V_1 are weight concentration, the density of the base fluid, density of nanoparticle, volume of lower and higher concentration of nanofluid, respectively. For the preparation of a hybrid nanofluid, equation (3) can be used to convert any concentration of nanoparticles by weight to the concentrations of one sample by

Table 1: Summary of mono synthetic- and organic-based nanofluids for thermal conductivity and dynamic viscosity research

Refs.	Type of nanoparticle	Name of nanoparticle	Base fluid	Size of nanoparticle (nm)	Concentration		Range of temperature (C)	Thermophy. prop.	k, μ influence
					ω	ϕ			
[57]	Metal	Cu	Oil	40–65	0.2–1	—	25–60	k, μ	Concentration, temperature
[185]	Metal	Ag	Oil	20	0.12–0.72	—	25–100	k	Concentration, temperature
[42]	Non-wood	Coconut fiber	W:EG 40:60	30–65	0.04–1	—	15–60	μ	Concentration, temperature
[193]	Metal oxide	Al_2O_3	Glycerol	20–100	—	1–5	20–70	μ	Concentration, size of nanoparticles, duration of ultrasonication, temperature
[148]	Carbon based	SiC	EG and PG	45–65	0.1–3	—	25–80	k, μ, electrical conductivity, σ	Concentration, temperature, base fluid
[155]	Carbon based	SiC	EG, PG, EG:W and PG:W	45–65	0.1–3	—	25–60	k	Concentration, temperature, base fluid
[89]	Carbon based	MWCNT	Water	OD = 7 nm ID = 2–5	—	0.1–0.5	25–60	k	Concentration, temperature
[173]	Carbon based	GO FGO	Water	Sheet size = 0.5–0.5 µm, thickness = few nm	0.01–0.1	—	23–40	k, μ	Concentration, temperature, functionalized derivative
[175]	Carbon based	GQD	W EG W:EG 60:40	20	—	0.05 –0.5	10–40	k, μ	Concentration, temperature
[198]	Carbon based	GO rGO	Water	Thin platelet sheets	—	0.0005–0.1	20, 30	μ	Concentration, shear rate
[40]	Non-wood	Palm kernel	W:EG 50:50 60:40	100	—	0.1–0.5	10–50	k, μ	Concentration, temperature, surfactant
[170]	Metal oxide	Al_2O_3	EG	8–282	—	1–4	31–136	k	Concentration, temperature, size of particles
[95]	Metal oxide	Al_2O_3	W:EG 60:40 50:50 40:60	13		0.2–1	30–70	k, μ	Concentration, temperature, base fluid
[165]	Metal and metal oxide	Cu Al_2O_3 and CuO	EG	10 35	—	0.01–0.05	25	k	Concentration, age of particle
[29]	Metal oxide	Al_2O_3 CuO	Water, HE-200 oil, duo-seal oil	3 36	—	0.01–0.05	25	k	Concentration, base fluid, type of nanoparticles

(*Continued*)

Table 1: *Continued*

Refs.	Type of nanoparticle	Name of nanoparticle	Base fluid	Size of nanoparticle (nm)	Concentration		Range of temperature (C)	Thermophy. prop.	k, μ influence
					ω	ϕ			
[166]	Metal and metal oxide	Cu Al_2O_3 and CuO	EG	10 35	—	0–6	25	k	Concentration, age of particles, surfactant
[128]	Metal oxide	TiO_2	Water	72–76	1–35	—	10–70	k, μ	Concentration, temperature
[96]	Metal oxide and carbon-based	CuO SiO C60 MWCNT	EG, oil, water	33 12 10 10–30	—	1	25	k	Base fluid, type of nanoparticles, and surfactant
[178]	Metal	Ag	Water	8.2–23.4	0.1–0.6 g	—	30–50	k	Size of particles and temperature
[161]	Metal oxide	ZnO TiO_2	Water	10–60 10–70	—	1–3	25	k, μ	Concentration, base fluid, size of nanoparticles
[164]	Metal oxide	CuO	EG	30–50	—	1–5	25	k	Concentration, surfactant
[169]	Metal oxide	Al_2O_3 CuO	Water	36 and 47 29	—	0.05–18	20–40	k	Concentration, temperature, size of particles
[38]	Wood-based nanoparticles	Mango bark	Water	100	0.1–0.5		10–60	k, μ	Concentration, temperature
[167]	Metal oxide	Al_2O_3 SiO_2 TiO_2	Methanol	13 5–15 21		0.005–0.15	1–20	k	Concentration, temperature
[177]	Carbon-based	MWCNT	Water	OD = 5–50 ID = 2–15		0.05	10–45	k, μ	Shape, size, and temperature
[145]	Non-wood	Rice bran	Water	50		0.1–3	25–55	k	Concentration, temperature
[16]	Wood-based	Cellulose nanocrystal (Canadian Hemlock tree)	W:EG 60:40	9–14	0.1–1.5	—	30–70	k, μ	Concentration, temperature
[190]	Carbon based	CNT	EG	60–100	0.12–0.4	—	25–60	k, μ	Concentration
[151]	Metal oxide	Al_2O_3	W:EG 80:20 60:40 40:60	36	0.3–1.5	—	20–60	k, μ	Concentration, temperature, base fluid
[182]	Metal oxide	Al_2O_3 TiO_2	W:EG 80:20	120 21	—	0–4	15–60	μ	Concentration, temperature

(*Continued*)

Table 1: *Continued*

Refs.	Type of nanoparticle	Name of nanoparticle	Base fluid	Size of nanoparticle (nm)	Concentration		Range of temperature (C)	Thermophy. prop.	k, μ influence
					ω	ϕ			
[184]	Metal oxide	ZnO	EG	10–20	—	0.002–5	10–60	k, μ	Concentration, settling time, temperature μ: Shear rate
[93]	Metal oxide	Al_2O_3	Water	15–50	0.02–0.15	—	25	k	pH, nanoparticles, and surfactant concentration

volume. equation (3) is used to prepare higher concentrations of nanofluid, followed by equation (4) which is used to prepare the other sample at a lower concentration by dilution.

Tables 1 and 2 describe mono- and hybrid synthetic- and organic-based nanofluids on thermal conductivity and viscosity investigations, respectively. The combinations of the two different types of nanoparticles may be between carbon-based and metal, carbon-based and metal oxide, carbon and organic-based, metal and metal, metal and metal oxide, or metal oxide and metal oxide. Reviews on hybrid nanofluids can be found in Sarkar *et al.* [76], Leong *et al.* [77], Babu *et al.* [54], Nabil *et al.* [78], Gupta *et al.* [79], Sajid and Ali [80], and Babar and Ali [81].

4 Morphological observation

Characteristic assessment is typically carried out after the nanofluids preparation to confirm the size of nanoparticles supplied by a manufacturer or laboratory-produced organic-based nanoparticles. It can be used to visualize the shape and structure of the nanofluid of mono-sized nanoparticles in the base fluid. This approach has also been used to imagine interactions of two or more types of nanoparticles in a hybrid nanofluid.

Sharifpur *et al.* [38] used SEM image to verify the size of mango bark particles found to be 100 nm. SEM is used to magnify detailed images of a material using a fine electron probe with an energy usually up to 40 keV [82]. The probe concentrates directly on the sample through a series of lenses and produces a focused beam on the sample's surface. A spectrum of signals is generated because of the reflection of the shooting electron, creating an image of the surface of a sample.

Nabil *et al.* [75], on the other hand, visualized the spherical shape of TiO_2 and SiO_2 by using a magnification ×140,000 and ×170,000, respectively by using TEM. TEM is used to describe the interaction of TiO_2 and SiO_2 as hybrid nanofluid. A magnification index of ×39,000 was used to picture the contribution of SiO_2 to fill the void between TiO_2 nanoparticles. This filling gap leads to a reduction in the distance between TiO_2 and an increase of 22.8% in thermal conductivity compared to W:EG 60:40%-based fluid.

Unlike SEM, TEM uses transmitted electrons passing through the sample to generate an image capable of obtaining information on the inner structure and composition of the sample [83]. Yarmand *et al.* [84] verified the laboratory-produced activated carbon from fruit bunch

Table 2: Summary of hybrid nanofluids for thermal conductivity and dynamic viscosity research

Refs.	Type of nanoparticle	Name of nanoparticle	Base fluid	Size of nanoparticle	Concentration		Range of temperature	Investigation	k, μ influence
					ω	ϕ			
[160]	Metal + carbon based	Ag + MWCNT	Water	MWCNT, D = 10–20 nm Ag, D < 35 nm	0.5–1	—	30–80	k	Concentration, temperature, surfactant
[91]	Metal oxide + carbon based	Fe_3O_4 + GE	Water	Fe_3O_4, D = 5 nm	0.001–1	—	20–40	k, μ	Concentration, temperature
[176]	Metal oxide + metal	TiO_2 + Ag	Water	TiO_2, D = 15 and 300 nm	1–3	—	15–40	k	Concentration, temperature
[156]	Carbon based + metal	CNT + Cu, CNT + Au	Water	CNT, D = 150–200 nm Au, D = 15 nm Cu, D = 35–50 nm	—	0.05–1	25	k	Concentration, settling time
[157]	Metal + carbon based	Cu + MWCNT	Water, EG	MWCNT, D = 25–30 nm Cu, D = 5–8 nm	—	0.006–0.03	30–48	k	Concentration, temperature
[162]	Metal + metal oxide	Cu + TiO_2	Water	55 nm	—	0.1–2	30–90	k	Concentration, temperature
[109]	Metal oxide + carbon based	TiO_2 + CNT	Water	TiO_2, D = 27 nm	0.1–0.2	—	25–40	k, μ	Concentration, temperature
[75]	Metal oxide + metal oxide	TiO_2 + SiO_2	W:EG	TiO_2, D = 50 nm 60:40	— SiO2, D = 22 nm	0.5–3	30–80	k, μ	Concentration, temperature
[92]	Metal + metal oxide	Cu + Cu_2O	Water	Cu – D = 200 nm Cu_2O – D < 30 nm	0.3 wt%	—	15–60	k	Temperature, size of grinding ball. Duration of grinding ball
[97]	Metal + carbon based	Ag + diamond	EG	10		0.005–0.1	10–60	k, μ, ρ	Concentration, temperature
[37]	Organic + carbon based	Clove buds + GE nanoplatelet	Water	GE nanoplatelet – Thickness: 2 nm, lateral size: 2 μm	0.03–0.1	—	20–50	k	Concentration temperature
[171]	Metal + metal oxide	Cu + Al_2O_3	Water	D = 77 nm	—	0.1–2	Room temp.	k, μ	Concentration, settling time μ, concentration & shear rate
[158]	Metal + carbon based	Ag + GE	Water	D = 2 μm	0.02–0.1	—	20–45	k, μ	Concentration, temperature
[159]	Metal + carbon based	Pt + GE	Water	—	0.02–0.1	—	30	k	Concentration

fibers added to GNP/EG nanofluids using TEM and field emission scanning electron microscopy (FESEM). Activated carbon has filled the GE sheet to boost the thermophysical properties and electrical properties of the EG-based fluid. Maximum thermal conductivity was reached by 6.47% at 40°C at a concentration of 0.06 wt%. Same as TEM, FESEM is used to envision very small (as small as 1 nm) topographic details of the surface, entire, or fractional material. However, the difference between FESEM, SEM, and TEM is the process of generation of electrons. FESEM oriented electrons in a high-vacuum column to create a scan beam [85]. These electrons, which were emitted from the field emission source, accelerated in the light electrical field gradient to emit secondary electrons from the sample. The angle and velocity of secondary electrons produce an electronic signal to the detector, which translates the signal as the surface structure of the material.

5 Stability measurement

After the dispersion of the particles in a base fluid was confirmed to be in the range of nano-sized (1–100 nm), the stability of the nanofluid should be established. The stabilization of nanofluids is vital because the properties of nanofluids depend on it [51,86]. Stability is defined by how long nanoparticles can be homogeneously suspended in the base fluid, low agglomerations, and free from chemical reactions with the base fluid [6]. Nevertheless, the stability of nanofluids may differ depending on ultrasonication. The ultrasonication method and time affect the size of nanoparticles, and optimum sonication time should be taken into account [72]. The increase in ultrasonication time will break down the aggregation of nanoparticles in the form of a large cluster by Brownian motion intensities [87]. Nonetheless, additional ultrasonic energy fused them again into a larger cluster due to high surface energy. Mahbubul *et al.* [88] reported that the ideal ultrasonication period for aqueous TiO_2 is 150 min. Asadi *et al.* [89] found that the maximum ultrasonication time for MWCNT/water was 60 min. The period which exceeds that duration deteriorates the stability. Sedimentation is another factor crucial to the stability of nanofluids [51]. A critical concentration of surfactants or a quantity of micell may be needed to prevent the rapid sedimentation of nanoparticles [72]. In addition to ultrasonication and the use of the surfactant, stirring time, the surface charge on nanoparticles, the pH of nanofluids, and the size of nanoparticles influence stability [51,90]. Stability can be measured both qualitatively and quantitatively.

5.1 Qualitative measurement

A qualitative method of sedimentation observation is the most common indicator of stability. Sedimentation occurs when there are two well-defined distinct phases of the supernatant liquid (clear liquid at the top) and slurry at the bottom. Barki *et al.* [70] tested the stability of aqueous mango bark nanofluid with no surfactant and three different types of surfactant. Observations of sedimentation were conducted after ultrasonicated for an hour. No settlement was observed after the sample was idle for two weeks for aqueous mango bark, aqueous mango bark with 10 wt% hexadecyltri methyl ammonia bromide ($C_{19}H_{42}B_rN$), and aqueous mango bark with lauric acid in all the sample concentrations ranging from 0.1 to 4 vol%. Settlement of some particles was observed when 10% of sodium dodecyl sulfate ($C_{12}H_{25}N_aO_4S$) was added to the sample. Askari *et al.* [91] observed a pH effect of 3, 5, 7, 8, and 10 on aqueous Fe_3O_2–GNP hybrid nanofluid. Samples were sonicated for 10 min after nanofluid preparation using a two-step method and 10 min after the pH modification. Hybrid nanoparticles with a pH value between 3 and 5 began to reagglomerate 10 min after preparation. Following one day of testing, the samples were utterly sedimented. On the other hand, the sample with a pH value of 7 is started to form two separate phases after two weeks of observation. It was sedimented entirely within one month of study. The pH values of nanofluid 8 and 10, on the other hand, were found to be stable after a month of idle exposure. Nevertheless, the author proposed that pH 8 aqueous Fe_3O_2/GE hybrid nanofluid be used for industrial applications as this pH is neutral. Nine *et al.* [92] argued that the synthesis of nanoparticles also impacted stability. Sedimentation varies depending on the size of the ball and the duration of the ball milling process of the raw micro-sized Cu particles to the nano-sized Cu_2O particles and Cu/Cu_2O cermets. The observation was conducted for 7 days, with an interval of 12 h. The findings show that the sample is stable when the sample is ground with 1 mm balls for 30 min and 3 mm balls for 60 min. When the ground time was extended for 90 min for both sizes of the balls, the stability of the nanofluid deteriorated.

5.2 Quantitative measurement

Many quantitative measurements can be used to determine stability. Among them, zeta potential analysis, ultraviolet-visible (UV-Vis) spectrophotometer, constant-temperature viscosity measurement, spectral analysis method, electron microscopy, and light scattering methods can be

used [16,51,93,94]. UV-Vis spectrophotometer is used to track the dynamics of the dispersion process. Sadri *et al.* [37] observed the dispersibility of clove-functionalized GNP in water by UV-Vis spectrophotometer relative to sedimentation time. The sedimentation magnitude is decreased for all concentrations on a day-to-day basis after the sample was prepared. Nevertheless, the value is constant after 45 days of preparation. Nabil *et al.* [75] measured the absorbance ratio to assess the impact of ultrasonication durations on sedimentation time for over 350 h. Chiam *et al.* [95] investigated the absorbance of Al_2O_3 in W:EG 60:40% by volume ratio for three different volume concentrations. Absorbance increased as the concentration increased for this nanofluid and reached a peak absorbance at the wavelength of 330 nm. This trend illustrated the rise in nanoparticle suspension as the concentration increases, which means that stability is preserved even at higher concentrations. The absorbance ratio, $\bar{A}_r$ was calculated as [95]:

$$\bar{A}_r = \frac{\bar{A}}{\bar{A}_o} \tag{5}$$

where $\bar{A}$ refers to the nanofluid absorbance and $\bar{A}_o$ refers to the base fluid absorbance. The absorbance ratio was 0.2 when the sample was not sonicated, and the value increased as sedimentation time increased. The absorbance ratio increased to 0.8 as the sonication time increased to 90 min indicating the most stable state of the sample. However, the absorbance ratio is again reduced to 0.7 as the sonication time is extended to 120 min, the same as the 60 min sonication time. Hwang *et al.* [96], Oliveira *et al.* [97], Bello *et al.* [98], and Zubir *et al.* [99] also used UV-Vis spectrophotometer to evaluate the stability of CNT and fullerene in refrigerant oil, diamond–Ag in EG, and coconut shell nanoparticles, respectively.

Zeta potential tests the repulsive force of two nanoparticles [51]. For a zeta potential index above ±60 mV, the stability of the nanofluid is excellent, and for a zeta potential below ±5 mV, the nanofluid is unstable [72,100]. Zeta potential was measured by Adewumi *et al.* [42] to assess the stability of coconut fiber carbon nanoparticles in W:EG 40:60% at four different concentrations. After one week of observation, the stability of these samples was visually unstable. Nevertheless, the zeta potential index for 0.04, 0.08, 0.5, and 1 wt% are 84.8, 130, 126, and 120 mV which have shown excellent stability. Zhu *et al.* [93], Selvam *et al.* [100], and Sedeh *et al.* [101] also used zeta potential to measure the stability of aqueous Al_2O_3, Ag in W:EG 70:30%, CuO and TiO_2 in ethanol and liquid paraffin, respectively. Besides that the pH of the sample can be altered to regulate the value of the zeta potential, which, as a result, controls the stability of nanofluids [72]. Nonetheless, Chiam *et al.* [95] recorded that pH shifts were only 5% when the concentration of Al_2O_3 rose from 0.2 to 1% when diluted in W:EG at 40:60% of the volume ratio. The lowest pH value is 5.34 when 1 vol% of Al_2O_3 is diluted in W:EG at 40:60%. The highest pH was obtained when W:EG was 50:50% without nanoparticle with a value of 5.67. Therefore, the pH shift is minimal and is assumed to be constant in the preparation of nanoparticles. Bouguerra *et al.* [102] noted, however, that the nanoparticles are strongly deagglomerated at pH between 4.5 and 6 for all concentrations. Nanoparticles provided a greater pH value of greater than 6.5 with larger agglomerated particles for all concentrations. The interpretation is that the nanofluid approached the isoelectric point (IEP) of Al_2O_3 at a pH range of 9.2–9.5 [90,103]. While most papers neglect the pH effect, it is crucial to ensure that the pH value of nanofluid is far removed from the IEP of the selected nanoparticles. It is necessary to ensure that the clustering of nanoparticles is minimized and that the nanofluid stability is maximized. Additional acids or bases are required to alter the pH of the IEP and improve its stability [104]. Okonkwo *et al.* [105] indicated that the pH of Al_2O_3 was more stable at a higher pH value of 12 and a lower concentration. Chavan and Pise [106] have modified the pH value of Al_2O_3, TiO_2, and SiO_2 to 6.4, 8.6, and 5.3 to ensure the pH values of Al_2O_3, TiO_2, and SiO_2 are varied from their IEP of 9.4, 5.8, and 2.3, respectively. Nevertheless, this necessity would create a conflict with the requirement to hold nanofluid at pH neutral to prevent oxidation and dissolution of nanoparticles [107].

6 Thermophysical properties

Nanofluid properties depend mainly on five parameters: thermophysical, heat transfer, particles matter, colloid, drag reduction, and lubrication [8]. Thermophysical properties include temperature, viscosity, density, thermal conductivity, specific heat, and enthalpy [49,100,108]. Heat convection, heat conduction, heat capacity, and the Prandtl and Nusselt number are dependent on heat transfer [109–111]. Particle-based parameters include size, shape, BET (surface area analysis), and crystalline phase [39,48,112]. Suspension stability, zeta potential, and pH value depend on colloidal properties [70,87,90]. Drag reduction properties include viscosity, pressure drop or pressure loss, friction factor, coefficient of friction, and wall shear stress [114–116]. The properties for lubrication are viscosity, viscosity index, friction coefficient, wear rate, and extreme pressure [117–119]. The thermophysical properties of

thermal conductivity and dynamic viscosity are chosen in this study to be explored in detail as these properties represent the thermal performance and flow of nanofluid.

6.1 Data comparison

In this study, the thermal conductivity and dynamic viscosity ratio of the various nanofluid investigations was compared and discussed. The effects of thermal conductivity and dynamic viscosity of mono and hybrid synthetic- and organic-based nanoparticles dispersed in different types of base fluids were then retrieved. Data extraction from graphs in the literature was exported using open-source software called Engauge Digitizer. The thermal conductivity analysis was sorted by the effect of the base fluid, types of nanoparticles and their concentration, temperature, and size of nanoparticles. On the other hand, dynamic viscosity comparison was sorted by the effect of concentration, temperature, and size of nanoparticles. As the literature has conducted various weight or volume concentrations, this study compared them using a normalized weight or volume concentration, C_N using the following equation:

Weight concentration:

$$C_N = \frac{\omega_{nf_i}}{\omega_{nf_{max}}} \tag{6}$$

Volume concentration:

$$C_N = \frac{\varphi_{nf_i}}{\varphi_{nf_{max}}} \tag{7}$$

where w_{nf_i} and φ_{nf_i} are the weight or volume concentration at respective concentration interval, $w_{nf_{max}}$ and $\varphi_{nf_{max}}$ are the maximum investigated weight and volume concentration of respective reference.

The thermal conductivity ratio, k_r, and dynamic viscosity ratio, μ_r, was calculated as follows:

$$k_r = \frac{k_{nf}}{k_{bf}} \tag{8}$$

$$\mu_r = \frac{\mu_{nf}}{\mu_{bf}} \tag{9}$$

The trend line of thermal conductivity and dynamic viscosity ratio for respective references were discussed and analyzed.

6.2 Thermal conductivity

Thermal conductivity emerges as the microstructure energy is transferred. As molecules move or vibrate at finite temperature, they collide or interact with energetic particles, transferring their kinetic energy to less energetic molecules. Most synthetic-based nanofluids are expected to have higher thermal conductivity compared to base fluids, as the thermal conductivity of nanoparticles is higher than that of base fluids [8,77].

The thermal conductivity of nanofluids can be influenced by 10 different factors: the type of base fluid, the type of nanoparticles, weight or volume concentration (quantity of nanoparticles), the temperature, the size and shape of nanoparticles, the average size of cluster nanoparticles, the stability, the surfactant, the acidity (pH), and aggregation [49,120–122]. Tlili *et al.* [123] proposed that in addition to the effects mentioned above, the alteration of the AR and the quality of nanoparticles may impact the thermal conductivity of nanofluids. In addition, carbon nanotube (CNT) performance is influenced by various factors, including the number of defects, morphology, atomic structure, and the presence of impurities. Ebrahimi *et al.* [124] added that the magnetic field and its strength could also alter the thermal conductivity for some nanofluids.

There are four different mechanisms of nanoparticles that influence the thermal conductivity of nanofluid in microscopic measurements, namely the formation of an interfacial layer between the base fluid and nanoparticles, the Brownian motion of nanoparticles, the nature of heat transfer in nanoparticles, and the clustering of nanoparticles [125–127]. The nanoscale particles primarily drive the Brownian motion of the particle's suspensions. The energy is transmitted through heat conduction between the moving nanoparticles and the heat convection between the nanoparticles and the base fluid [126,128,129]. As the temperature of the solution increases, the intermolecular bond in the fluid layer decreases. At the same time, nanoparticles are highly translated, rotated, and shifted around randomly. As a result, the interaction between micro-liquids and nanoparticles increases the nanofluid's thermal conductivity [95]. Brownian motion is responsible for transporting energy *via* collisions between nanoparticles and micro-liquid convection, mixing, and enhancing the transport of thermal energy [68].

The interfacial solid-like structure, called nanolayer, formed in the form of a layer of liquid molecule near the surface of nanoparticles, plays an effective role in the thermal conductivity of nanofluids [130,131]. This interfacial nanolayer effect of heat transfer was negligible for the micro-sized particles in the base fluid because the thickness was too small relative to the diameter of the particles. However, in nano-sized particle suspensions, this thickness cannot be overlooked because the thickness

of this layer, which behaves like a solid, is in a magnitude of a nanometer. The effect of nanolayer in balance as nano-sized particles is smaller because heat transfer is more effective when the nanolayer thickness is wider. Thermal conductivity increases as the nanolayer thickness increases [130,132,133].

Besides, numerous studies have investigated the impact of clustering and alignment of nanoparticles on thermal conductivity [134]. Based on the analysis conducted by Esfe *et al.* [120], the thermal conductivity of nanofluids may be enhanced or degraded by the formation of nanoparticle alignment or clustering. Zhu and Zhang [134] found an abnormal function of Fe_3O_4 in water as the volume fraction increased. Nanoparticles of Fe_3O_4 were in the form of alignments and small, loose clusters at low concentrations. The number and length of alignments and clusters increase as the concentration increases. They observed a sharp increase in the thermal conductivity of nanofluids as the concentration increased. Interestingly, the thermal conductivity ratio of Fe_3O_4/water is higher than the aqueous nanofluid of Al_2O_3, CuO, and TiO_2, even though the thermal conductivity of individual nanoparticles is higher than that of Fe_3O_4. They believe that other nanoparticles have not displayed the same alignment and clustering characteristic as Fe_3O_4 does. Megatif *et al.* [109] also found a positive effect of thermal conductivity of TiO_2-CNT by an increase of 2.5% in the thermal conductivity of hybrid nanofluid relative to CNT nanofluid. Jiang *et al.* [32] believe that a chain-like aggregation of CNT forms a conductive path that improves thermal conductivity performance. The rise was 20.5% for the hybrid nanofluid compared to the water-based fluid at 25°C [109].

The next one is the thermal transport mechanism for nanoparticles by photon and electron heat transfer [135,136]. The increase of thermal conductivity in the presence of nanoparticles exists at a molecular level due to the efficient motion of liquid atoms. Sarkar and Selvam [135] argued that nanofluid motions are ballistic rather than diffuse, which is the nature of nanoparticles. He clarified that the increase of 1 wt% of Cu nanofluid surrounded the liquid atom 28 times faster than that of Cu nanoparticles, which induced higher thermal conductivity of nanofluid. The thermal conductivity measurement was carried out using a green-Kubo method to investigate the ability of nanofluid molecular dynamics to predict thermal conductivity at the atomic level. Avsec [137] supported the claim in the light of the numerical analysis evidence that explained an invalid assumption of the effect of thermal conductivity on heat transport *via* diffuse but ballistic phenomena. In addition to the mechanism pointed above, Iacobazzi *et al.* [138] introduced two additional mechanisms influencing thermal conductivity, *i.e.*, thermal boundary resistance and mass difference scattering.

The thermal conductivity of mono-nanofluid has been thoroughly studied and debated in the literature [7,57,122,126,139,140]. The thermal conductivity review for hybrid nanoparticles can be referred to in refs. [28,68,77–80]. Thermal conductivity models can be reviewed in refs. [126,141,142]. This section will address the effect of different types of nanoparticles and base fluids, nanofluids concentrations, bulk temperature, and particle size on thermal conductivity.

6.2.1 Effect of a base fluid

Figure 2 shows the standard thermal conductivity data for water, W:EG mixtures, W:PG, EG, and PG chosen to be compared with experimental results. Standard thermal conductivity data for water were obtained from the

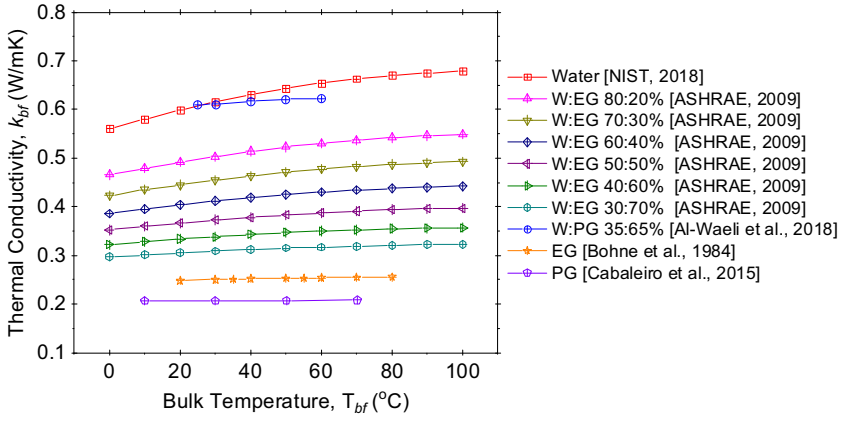

Figure 2: Thermal conductivity of conventional base fluids.

thermophysical properties of fluids system webbook issued by the National Institute of Standards and Technology, U.S. Department of Commerce [143]. The thermal conductivity of water and EG mixture was derived from ANSI/ASHRAE Standards for Ventilation System Design and Acceptable Indoor Quality [144]. The results obtained from the experiment compared with the standard thermal conductivity data are essential to test the reliability of the experimental setup and the results [75,94,96,99,145]. For most investigations, water-based fluid is the preferred choice since it is neutral to most synthetic-based nanoparticles at temperatures below 100°C, is the most convenient fluid, and easy to handle in the laboratory. The EG-based fluid is the primary option for the researcher to add low-pressure coolant to the engine. W:EG mixture-based fluid is used in high-temperature applications.

A few studies have been conducted to identify base fluids that function well with selected synthetic-based nanoparticles. Cabaleiro *et al.* [146] reported the effect of EG and PG on TiO_2 nanoparticles dispersion with two different nanocrystalline structures. The result revealed that the thermal conductivity of TiO_2/PG with lower thermal conductivity of base fluid than EG has a superior enhancement at all concentrations from 5 to 25 wt% at the same temperature compared to TiO_2/EG. The thermal conductivity of EG and PG is 0.248 and 0.207 $W\,m^{-1}\,K^{-1}$ at 30°C, respectively. These results are consistent with those of Moosavi *et al.* [147]. Moosavi *et al.* [147] found that the thermal conductivity enhancement of ZnO at a lower thermal conductivity of EG was higher, with 10.5% than glycerol (G) with 7.2% at 3 vol%. The thermal conductivity of EG and G is 0.250 and 0.280 $W\,m^{-1}\,K^{-1}$, at the same temperature, respectively. However, these results are refuted by the findings of Akilu *et al.* [148]. Akilu *et al.* [148] compared the thermal conductivity of EG and PG-based β-SiC nanofluid. The maximum relative thermal conductivity of 1 vol% of β-SiC nanofluid at 25°C is 5.5% for EG-based nanofluid compared to PG-based nanofluid with 2.9%. The result presented does not infer that the thermal conductivity enhancement of nanofluid is increased linearly with the thermal conductivity of the base fluid.

On the other hand, Sonawane *et al.* [149] considered water, EG, and paraffin oil with TiO_2 dispersion and found that TiO_2 dispersed in water with the lowest dynamic viscosity (0.806 mPa s) had the highest percentage of increase in thermal conductivity compared to EG (16.5 mPa s) and paraffin oil (30 mPa s). They explained that the lower viscosity of the base fluid has led to an improvement in the thermal conductivity of nanofluid because low viscosity of base fluid allows particles to interact more easily with each other, leading to an improvement in the Brownian motion of nanoparticles in fluids. It corresponds to further particle-to-particle interactions over a given time. As a result, TiO_2 nanoparticles can transfer heat more effectively to water than EG and paraffin oil. Nevertheless, despite the mechanism described, the lower enhancement was provided by TiO_2/EG instead of TiO_2/paraffin oil, which is contradicted by the observation that EG does not have the lowest viscosity in the group. Also, the thermal conductivity of all base fluids was optimally increased after 60 min of ultrasonication. After 60 min, the thermal conductivity performance of both nanofluids was slowly reduced.

However, the effect of ultrasonication time gave the opposite result to the previous work of Codreanu *et al.* [150]. The effect of water and EG-based fluid on Fe–C nanoparticles dispersion before and after ultrasonication has been investigated. Thermal conductivity improved by 35.3% without ultrasonication for Fe–C/water at 1 vol%. Percentages of thermal conductivity enhancement were reduced linearly to 28.9% after 7 h of ultrasonication. On the other hand, Fe–C/EG trend line at the concentration of 0.25 vol% was not equivalent to Fe–C/water. Maximum thermal conductivity enhancement was 24.1% before ultrasonication decreased after an hour of ultrasonication. However, the thermal conductivity was restored as the duration of ultrasonication increased until it reached 40.1% after 7 h. The explanation for this trend is that nanoparticles formed a unique cluster of nanoparticles with specific base fluids. When the Fe–C nanoparticles were dispersed in deionized water, the nanoparticles formed a cluster of uniform downy mass where they were rapidly settled. These clusters may not significantly affect particle size, although the cluster of Fe–C/water nanoparticles has decreased from 474.8 to 3–6 nm. On the other hand, when dispersed in EG, nanoparticles are formed in a uniform, small, compact cluster. The magnitude of Fe–C/EG nanoparticle cluster decreased from 101.6 nm to less than 10–24 nm after ultrasonication had a substantial impact on the improvement of thermal conductivity.

In addition to selecting a single type of base fluid for nanofluid analysis, research was also performed for the optimum percentage of mixtures of two different types of the base fluid. Sundar *et al.* [151] analyzed Al_2O_3 in water and EG mixture at three different weight concentrations. The test was conducted at 40:60, 60:40, and 80:20% by weight of W:EG with a volume concentration of 0.3–1.5% and a temperature between 20 and 60°C. Maximum thermal conductivity increase is 32.26% at a concentration of 1.5 vol% with W:EG 80:20% at the temperature of

60°C. The thermal conductivity of nanofluid is higher as the weight concentration of EG is lower. This research discovery is similar to the work done by Chiam *et al.* [95] using the same nanoparticles of Al_2O_3. Al_2O_3 nanoparticles with an average size of 13 nm were dispersed in three different volume ratios of W:EG of 40:60, 50:50, and 60:40%. The authors found that the highest thermal conductivity value increased with an increase in the water ratio. Thermal conductivity peaked at 12.8% with 1 vol% of Al_2O_3 at 60:40% of W:EG. The higher the amount of EG added to the water, the lower the percentage of the water and lower the thermal conductivity of the mixture.

Some studies have opted to use W:EG mixture at various volume ratios for their applications. Vajjha *et al.* [152] used a mixture of W:EG 40:60% by weight to investigate the thermophysical properties of the three different types of nanoparticles, Al_2O_3, CuO, and SiO_2. The usage of this percentage of the W:EG mixture is because it is widely used as a heat transfer fluid in the cold region of the world in building heaters and in automotive radiators. Timofeeva *et al.* [153] used the W:EG 50:50% volume ratio to evaluate the thermal conductivity, viscosity, and heat transfer coefficient of SiC nanoparticles at four different sizes. This mixture was used for cooling in transport and power electronics. The thermal conductivity increased by 4–5% when dispersed in W:EG 50:50% at the same concentration and size. This effect cannot be explained simply by the lower thermal conductivity of W:EG-based fluid since the difference in improvement values predicted from the effective medium theory is less than 0.1%. It is most correlated with the lower value of the interfacial thermal resistance in W:EG nanofluids. Xie *et al.* [154] used W:EG 55:45% by volume percentage to examine four different nanoparticles with the same diameter size of 30 ± 5 nm for their heat transfer behavior. This mixture was used since it was widely used in engine cooling and solar energy systems. Among Al_2O_3, ZnO, TiO_2, and MgO nanoparticles, MgO nanoparticles have improved thermal conductivity by 4.5% at the concentration of 0.1 vol%. Al-Waeli *et al.* [155] found that W:EG and W:PG at the same volume ratio of 65:35% did not show substantial improvements in thermal conductivity at the same concentration and temperature even though W:EG and W:PG had a notable increase in viscosity and density

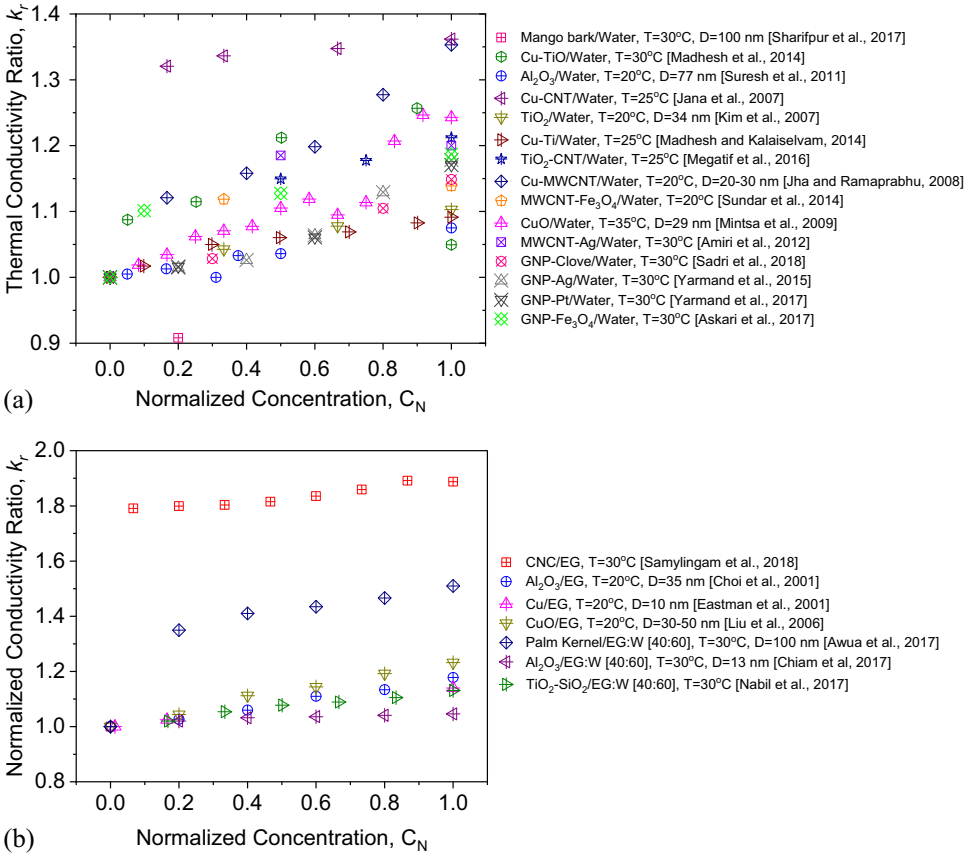

Figure 3: Effect of types of nanoparticles: (a) water (b) EG and W:EG 60:40%.

relative to the water-based fluid. Nano-SiC with a diameter of 45–65 nm with the aid of a surfactant is used for its thermo-physical properties to determine the best base fluid to be used in the photovoltaic/thermal system. The result was that both SiC/W:EG and SiC/W:PG with 0.5 wt% increase the thermal conductivity by just 1.66% at 25°C relative to the conventional water-based fluid.

6.2.2 Effect of types of nanoparticles

Figure 3 compared various types of nanoparticles dispersed in selected base fluids for nanofluid investigations. Synthetic- and organic-based mono- and hybrid-based nanoparticles have been dispersed in the base fluid of water, EG, and W:EG 60:40% to increase the thermal conductivity of the respective base fluid. As shown in Figure 3(a), the comparisons of 15 different types of water-based nanofluids were selected to compare the efficacy of selected nanoparticles in improving thermal conductivity. This distinction was made for nanoparticle dispersion in the water-based fluid at temperatures ranging from 20 to 35°C with thermal conductivity of water reduced from 1.0016 to 0.7193 mPa s, respectively [143]. Other effects that influence thermal conductivity, such as the size of nanoparticles, are considered not to be affected by this relationship. Overall, the thermal conductivity ratio increased with an increase in the normalized weight or volume concentrations. The maximum thermal conductivity ratio with aqueous Cu–CNT hybrid nanofluid can be seen as thermal conductivity increased by 36.2% at a volume concentration of 0.3% [156]. However, Jha and Ramaprabhu [157] just needed 0.03 vol% of aqueous Cu–MWCNT nanofluids to increase thermal conductivity by a little less than Cu–CNT dispersion by 35.3%. Conversely, aqueous mango bark decreased the thermal conductivity performance of water by 46% at a weight concentration of 0.5% [38]. Other aqueous nanofluids have improved thermal conductivity by less than 20%. GNP hybrid nanofluids with clove [37], Ag [158], and platinum [159] were investigated at concentrations ranging from 0 to 0.1 wt% with maximum thermal conductivity at 17.8%. Amiri *et al.* [160] and Askari *et al.* [91] measured aqueous MWCNT–Ag and GNP–Fe_2O_3 with a maximum weight concentration of 1% and maximum thermal conductivity improved by 20%. The addition of other nanoparticles may or may not increase the thermal conductivity of water-based fluid. Kim *et al.* [161] investigated mono-nanofluid of aqueous TiO_2 at a volume concentration of 1–3%, where the maximum increase in thermal conductivity is 10.3%. Then, Megatif *et al.* [109] applied CNT in aqueous TiO_2 at a concentration range of 0.1–0.2 vol% to increase the thermal conductivity by up to 21.2% relative to the base fluid. Conversely, Madhesh *et al.* [162] lowered the aqueous TiO performance by 2.2% by adding Cu with 2 vol%. This comparison demonstrated that the proposed carbon-based nanofluid to aqueous metal or metal oxide nanofluid would increase the thermal conductivity of mono-based nanofluid.

On the other hand, a comparison of different types of mono and hybrid nanoparticle dispersion in EG and a mixture of W:EG at a constant volume ratio of 60:40% is shown in Figure 3(b). There is a significant volume ratio of a mixture of W:EG in the literature. Even so, as mentioned in the previous section, a constant ratio of W:EG 60:40% was selected for this comparison, as this ratio was considered to have the most excellent performance relative to other volume ratios [16,75,95,163]. Samylingam *et al.* [16] used this base fluid mixture to increase their thermal conductivity by dispersing cellulose nanocrystal. Thermal conductivity was increased by 10% from a weight concentration of 0.001–0.015%, with the maximum thermal conductivity ratio of 1.89 achieved by a weight concentration of 0.013%. The second highest increase in thermal conductivity of W:EG 60:40%-based nanofluids is the dispersion of palm kernel nanoparticles reported by Awua *et al.* [40]. The maximum increase of 51% was achieved at 0.5 vol%. Other nanofluids improved thermal conductivity by ±20%. The maximum thermal conductivity for synthetic-based nanofluids exceeded 23.2% with the dispersion of 5 vol% of CuO in EG by Liu *et al.* [164] and the minimum thermal conductivity was achieved by Chiam *et al.* [95] with an improvement of 4.6% with the concentration of Al_2O_3 of 1 vol% in W:EG 60:40%. With the same type of nanoparticle of Al_2O_3 at a very low concentration of 0.05 vol% in EG, Choi *et al.* [165], however, achieved higher thermal conductivity enhancement by 17%. Nevertheless, Al_2O_3 was dispersed at a larger nanoparticle size, which therefore had a higher thermal conductivity. The effect of nanoparticle size is discussed in Section 6.2.5. Eastman *et al.* [166] and Nabil *et al.* [75] obtained a significant improvement in thermal conductivity by 13% when dispersing their selected nanoparticles in the base fluid. Nabil *et al.* [75] dispersed TiO_2–SiO_2 hybrid nanofluid at a concentration of 3 vol% in W:EG 60:40% of the base fluid, and Eastman *et al.* [166] dispersed Cu at a lower volume concentration of 0.5% in EG.

Mostafizul *et al.* [167] have dispersed three different types of nanoparticles, Al_2O_3, SiO_2, and TiO_2 in methanol with a maximum study concentration of 0.15 vol%. He documented that Al_2O_3 had the most remarkable improvement and that SiO_2 had the lowest increase in

thermal conductivity in methanol. The possible reason is that all nanoparticles have different individual thermal conductivity. These nanoparticles travel using the Brownian motion, where they translate, rotate, and shift to various degree based on their fundamental thermal properties.

6.2.3 Effect of concentrations

Figure 4 shows the effect of normalized weight or volume concentrations on the thermal conductivity ratio of four most favoured types of synthetic nanoparticles, Al_2O_3, Cu-based nanoparticles, Ti-based nanoparticles, and carbon-based nanoparticles dispersed in three different types of base fluids. Since these data given are normalized, the minimum and maximum examined concentrations for each reference may be found in Tables 1 and 2. These nanofluids were compared for the temperature range from 20 to 30°C where the increase in thermal conductivity of water, EG, and W:EG 60:40% is 2.8% [143], 0.2% [168], and 2% [144], respectively. The effect of nanoparticle size is neglected, and all selected nanofluids did not use any surfactant or pH adjustment for the stability in the sample. The pH value was retained as a neutral pH. In general, the thermal conductivity of all nanofluids was enhanced as the concentration increased. The figure shows that in all types of base fluids, CuO and Al_2O_3 nanofluids have a higher thermal conductivity ratio than other nanofluids. When the concentration increases, the distance between the nanoparticles decreases as the particles bang into each other more often, increasing the frequency of the lattice vibration that opens the possibility of heat transfer between the particles.

In Figure 4(a), Al_2O_3 was dispersed in four different base fluids, including water, EG, W:EG 60:40%, and methanol as extracted from the literature. There are three different diameters of Al_2O_3 used in the compared literature: 12–13, 35–36, and 77 nm. Eastman *et al.* [29, 166] and Sundar *et al.* [151] dispersed 35–36 nm of Al_2O_3 in water, EG, and W:EG 60:40% at 20°C. The maximum thermal conductivity ratio for these references is 1.29, 1.18, and 1.11 at the volume concentration of 0.01–0.05%, 1–5%, and 0.3–1.5%, respectively. Mintsa *et al.* [169] tested the same sample as Choi *et al.* at 25°C and obtained a significantly lower thermal conductivity ratio by 3%. Nevertheless,

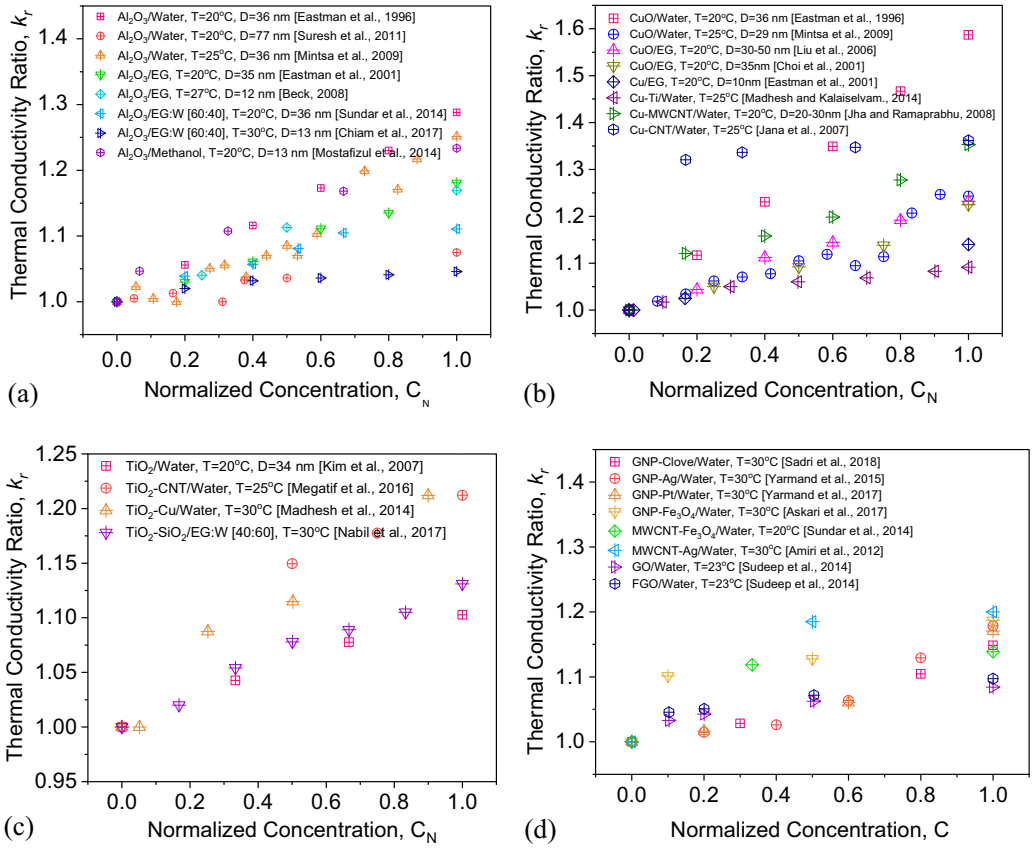

Figure 4: Effect of nanoparticle's concentration on thermal conductivity: (a) Al_2O_3, (b) Cu and CuO, (c) TiO_2, and (d) carbon based.

the maximum thermal conductivity ratio was reached by a volume concentration of 18% of Al_2O_3. Mostafizul *et al.* [167], Beck *et al.* [170], and Chiam *et al.* [95] investigated Al_2O_3 with a diameter of 12–13 nm at a temperature of 20, 27, and 30°C, respectively. The nanoparticle was dispersed in methanol, EG, and W:EG 60:40%, where the maximum thermal conductivity ratio for these comparisons is 1.23, 1.17, and 1.05, respectively. It was investigated at the concentrations of 0.01–0.15, 1–4, and 0.2–1 vol%, respectively. Suresh *et al.* [171] investigated aqueous Al_2O_3 with a diameter of 77 nm at the temperature of 20°C. The thermal conductivity ratio improved from 1.005 to 1.075, with Al_2O_3 dispersion of 0.1–2 vol%.

On the other hand, a comparison of different Cu-based nanoparticles homogeneously dispersed in water or EG was shown in Figure 4(b). CuO was dispersed in water and EG at a temperature range of 20–25°C and a diameter of about 29–50 nm. Eastman *et al.* [29] and Choi *et al.* [165] dispersed CuO with a diameter of 35–36 nm at 20°C with a concentration range between 0.01 and 0.05 vol%. CuO raises the thermal conductivity of water by 59% with a concentration of 0.05%, and a lower thermal conductivity was reached by EG by 23% at a concentration of 0.04%. Liu *et al.* [164] and Mintsa *et al.* [169] studied CuO in EG and water at higher concentrations. Liu *et al.* [164] examined CuO with a diameter of 30–50 nm dispersed at 20°C in water. Thermal conductivity improved by 23% with a concentration of 5 vol%. The increment percentage is the same for CuO/water nanofluid investigated by Mintsa *et al.* [169] at 12 vol% with a slightly smaller CuO of 29 nm at 25°C. On the other hand, Eastman *et al.* [166] performed a mono-Cu dispersed experiment in EG where thermal conductivity increased by up to 14% at a concentration of 0.5 vol%. Jana *et al.* [156] and Jha *et al.* [157] mixed Cu with CNT and MWCNT dispersed in a water-based fluid. The thermal conductivity ratio of both hybrid nanofluids increased by about 36% as the normalized concentration increased.

In addition to Cu–CNT nanofluid, Jana *et al.* [156] also examined the efficacy of Au in CNT/water nanofluid. Ironically, the thermal conductivity of hybrid nanoparticles has decreased the thermal conductivity of mono-nanofluid rather than increased as desired for hybrid nanofluid. The normalized thermal conductivity of CNT was then plotted to the volume concentration. The result showed that the thermal conductivity is non-linear to the volume concentration. The justification for this is that CNT, which has a broad AR of geometrical anisotropy, contributed to the anisotropic physical movement of interfacial thermal resistance. As the concentration increased, the loading of nanofluids increased, increasing the agglomeration where the final shape and size of nanoparticles in nanofluids become uncertain. On the other hand, Jha *et al.* [157] reported that Cu performed well with MWCNT when dispersed in water. Functionalized MWCNT processed the MWCNT, and the Cu–MWCT was synthesized by chemical reduction, which led to the discovery of more hydrophilic MWCNT. The higher the concentrations, these nanoparticles strengthen the working synergy between them, where Cu is homogeneously decorated in MWCNT and enhances the heat conduction between nanoparticles. This mechanism is not surprising, as several factors may have contributed to this discrepancy, as described earlier in this study.

The dispersion of mono and hybrid TiO_2 nanoparticles in water is compared in Figure 4(c). The comparison was made at a temperature range between 20 and 30°C. The thermal conductivity of TiO_2 nanoparticles in water increased from 4.3 to 10.3% as the volume concentration increased from 1 to 3% [161]. A slight increase in thermal conductivity was observed when SiO_2 was added to the TiO_2 nanofluid in W:EG 60:40% by volume ratio at all normalized volume concentrations. The thermal conductivity of TiO_2–SiO_2/W:EG 60:40% was increased by 3% at 3 vol% compared to mono TiO_2/water by Kim *et al.* [161]. Maximum improvement was obtained by adding Cu and CNT to TiO_2/water by 25.7 and 21.2%, respectively. Madhesh *et al.* [162] and Megatif *et al.* [109] have dispersed the maximum concentration of 2 and 0.2 vol% of their selected hybrid nanoparticles in the water-based fluid. Madhesh *et al.* [162] explained that there is more than one factor to the increase in thermal conductivity as the volume concentration increased. In addition to the chaotic Brownian motion of nanoparticles and the morphology of nanoparticles, the exposure of highly crystalline and heat conductive Cu nanoparticles to TiO_2 has laid the foundation for a thermal interface network between their microstructures and the fluid layers. Megatif *et al.* [109] found that 0.1 wt% of TiO_2–CNT hybrid nanoparticles had lower thermal conductivity than mono-CNT nanoparticles in the water-based nanofluid. CNT/water at 0.1 wt% is marginally higher than the hybrid TIO_2–CNT/water at 0.15 wt%. Hybrid TiO_2–CNT nanofluid surpasses the thermal conductivity of mono-CNT/water when the hybrid nanoparticle is 0.2 wt%. The thermal conductivity of TiO_2–CNT/water nanofluid at 0.2 wt% was increased by 3% compared with CNT/water nanofluid at 0.1 wt%. The rationale is that it could be due to the nanoparticles' agglomeration potential that led to the clustering effect between TiO_2 and CNT that contributes to the lower thermal conductivity of the hybrid nanofluid.

Carbon-based nanofluid required a technique involving non-covalent and covalent functionalization or mixed with metal or metal oxide to achieve high dispersion of carbon atoms which then increase the thermal properties of the base fluid. The covalent functionalization of carbon-based nanoparticles is related to the carbon-based molecular structure *via* the formation of covalent bonds [172]. New nanoparticle mixed in carbon-based nanofluid that shares at least one pair of electrons is claimed to have covalent functionalization with the carbon-based nanoparticles. Covalent functionalization helps improve the dispersibility, processability, and reactivity of carbon-based nanoparticles. Therefore, Figure 4(d) compared the thermal conductivity ratio of six different carbon-based hybrid nanoparticles to metal or metal oxide, GO, and FGO at 20–30°C. Like other types of synthetic-based nanofluid, the thermal conductivity ratio is increased as the carbon-based hybrid nanofluids increases. The GNT-clove/water [37], GNP–Ag/water [158], GNP-Pt/water [159], GO/water [173], and FGO/water [173] were investigated at the same highest concentration of 0.1 wt%. Comparing these five nanofluids, the sequence of highest thermal conductivity ratio is GNP–Ag/water > GNP-Pt/water > GNT-clove/water > FGO/water > GO/water. The GNT–Fe_2O_3 [91] and MWCNT–Ag [160] was investigated at the highest concentration of 1 wt% and MWCNT-Fe_2O_3 [174] by 0.3 wt%. The GNP–Ag/water with 0.1 wt% has the thermal conductivity ratio 3% lower than MWCNT/Ag/water with 1 wt%. This result shows with the same Ag/water nanofluid, the mixture of GNP in Ag–water gives better thermal conductivity enhancement than MWCNT.

Close attention needs to be paid to the hybrid nanofluid of the synthetic and organic mixture of GNT and cloves studied by Sadri *et al.* [37]. GNT-clove/water nanofluid increased thermal conductivity by 14.9% at a concentration of 0.1% by weight. Clove was selected as an effective organic nanoparticle to boost thermal conductivity as this source can enhance the functionality of GNPs in water. In addition, it has also contributed to environmental sustainability and cost-effectiveness, as it is one of the most grown spices in tropical climate regions. Although the dynamic viscosity of GNT-clove is like the base water, the thermal conductivity reached a maximum of 22.92% at 45°C for 0.1 wt% of nanoparticles.

6.2.4 Effect of bulk temperature

Although the nanofluid analysis is mostly about the effect of concentration, the relative change in thermal conductivity when nanofluids are dispersed in a base fluid is based on the experiment's initial temperature state. Most of the paper stated that the investigation was conducted at room temperature. However, the room temperature varies depending on the location of the lab, the humidity within the laboratory, and the weather of the region or country. It is often more convenient to mention the value of room temperature. Figure 5 describes the effect of bulk temperature on the thermal conductivity ratio of various mono and hybrid nanoparticles dispersed in water or a 60:40% by volume ratio of W:EG. The comparison was performed at the same concentrations of 1 wt % or 1 vol% for metal and metal oxide nanofluids and 0.1 wt% or 0.1% for GE nanofluids, where no surfactant drives the stability. Just like the previous comparison, in this comparison, the effect of nanoparticle size is ignored. All nanofluids have improved their thermal conductivity above the thermal conductivity of the base fluid. As shown in both figures, thermal conductivity ratio is increased as temperature increases for Ag–water [160], Ag-MWCNT/water [160], Fe_2O_3–water [91], Fe_3O_4–GNP/water [91], TiO_2-Cu/water [162], GO/water [173], FGO/water [173], GQD/water [175], Al_2O_3/W:EG 60:40% [95,151], and TiO_2–SiO_2/W:EG 60:40% [75]. On the other hand, the thermal conductivity ratio for TiO_2/water [176] and TiO_2–Ag/water [176] decreases as the temperature increases from 18 to 40°C.

Figure 5(a) shows the maximum thermal conductivity ratio was increased by 30% for Ag-MWCNT/water hybrid nanoparticle compared to the base fluid and increased by double compared to Ag–water at 80°C [160]. In the same research, MWCNT hybrid nanofluids with cysteine (Cys) and gum Arabic (GA) was also investigated for a concentration of 0.5 wt% in the temperature range of 30–80°C. The result shows that the thermal conductivity increment sequence is MWCNT-Ag/water > MWCNT-Cys/water > MWCNT-GA/water > Ag/water. The MWCNT developed a liquid layer interface that results in a higher thermal conductivity than that of the base fluid. With the addition of synthetic nanoparticles mixed in aqueous MWCNT, the nature of the covalent functionalization by Cys and Ag ions attached to the MWCNT surface has increased thermal conductivity. In contrast, GA is a non-covalent functionalization water-based MWCNT. Since Ag has a higher thermal conductivity than cysteine, the thermal conductivity of MWCNT-Ag is higher than MWCNT-Cys/water.

In Figure 5(a), particular emphasis should be addressed to the temperature of 40°C, where most of the mentioned references tested their nanofluids. Fe_3O_4–GNP/water has the highest thermal conductivity ratio with 1 wt%, followed by GQD/water with 0.1 vol%, and so on. These data show that GQD/water has a thermal conductivity ratio difference of just 4% when the concentration is 90% less than Fe_3O_4–GNP/water. As the concentration of GQD/water increased to

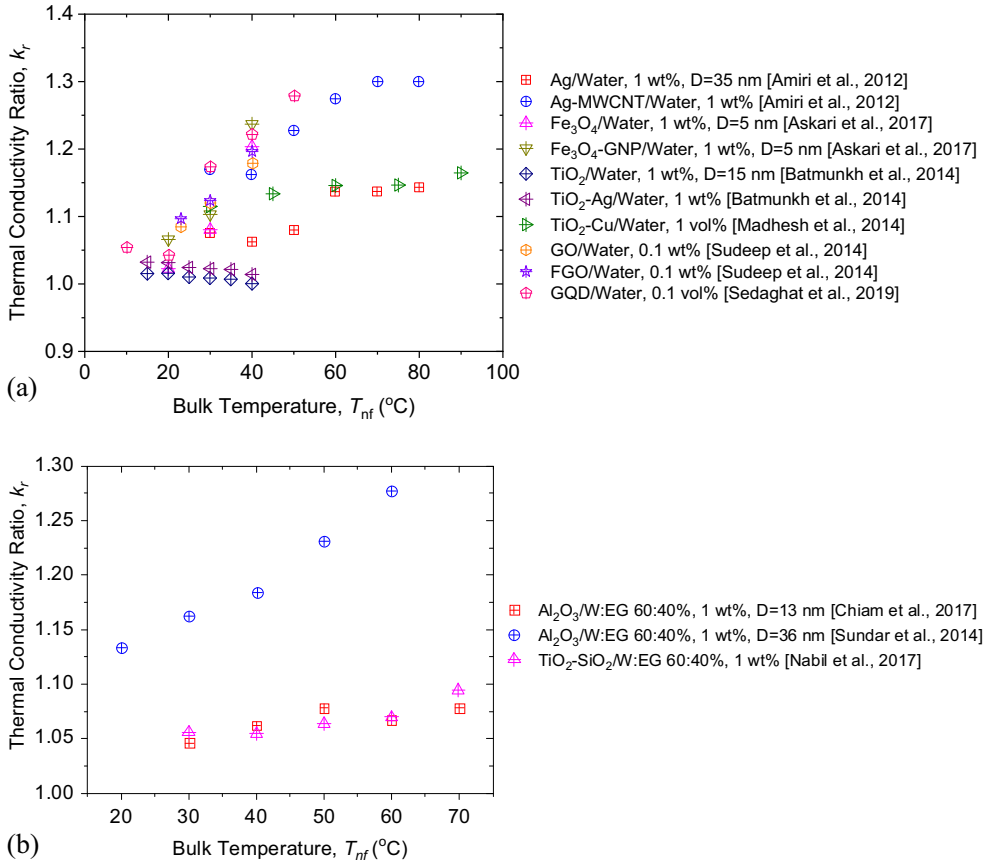

Figure 5: Effect of bulk temperature: (a) water and (b) W:EG 60:40%.

0.5 vol%, the thermal conductivity ratio climbed to 1.40. With a 50% lower concentration than Fe_3O_4–GNP/water, the increment in thermal conductivity ratio is 17% higher than Fe_3O_4–GNP/water. The reason for this is that GQD was synthesized using a zero-dimension carbon material with a diameter of 20 nm made from GE and carbon dots. It is chemically stable and has a larger surface area than other nanoparticles, resulting in higher surface properties and an increase in thermal conductivity. Like GQD/water, the thermal conductivity ratios of GO and FGO/water at 0.1 wt% are higher than hybrid Ag-MWCNT/water at 1 wt%. GO and FGO are oxidized and doped GE, respectively, with a modified plane hybrid of two and three single-bond carbon atoms (sp2 and sp3) with added functional groups to improve physical and chemical properties. GO is dispersible in practically all polar and nonpolar liquids, which increases the Brownian motion between carbon atoms. Even though the GO and the FGO are equal in size, structure, and morphology, the FGO/water data are higher than the GO/water. The reason for this is that adding fluorine (F) to GO alters the local environment surrounding the carbon atoms due to the strong electronegative nature of F- by producing extra sp3 and expanding the bandgap between carbon atoms which contributes to thermal enhancement.

Furthermore, at 40°C, the maximum thermal conductivity ratio is Fe_3O_4–GNP/water at 1 wt%. Askari *et al.* [91] investigated the effect of Fe_3O_4–GNP/water hybrid nanofluid compared to Fe_3O_4/water. At 20°C, the thermal conductivity of Fe_3O_4–water increased by only 2.3%. Adding GNP increases the value by 4.3–6.6% at the same temperature. As the temperature rises to 40°C, the thermal conductivity ratio of hybrid nanofluid rises by 3.3% to 1.24 compared to mono Fe_3O_4–water at the same temperature. The thermal conductivity of GNP is higher than that of Fe_3O_4, which contributed to the increase in aqueous Fe_3O_4–GNP hybrid nanofluid. As the temperature increases, the inter-particles and inter-molecular adhesion forces between Fe_3O_4 and GNP are weaker, resulting in an increase in random and Brownian motion that has contributed to the improvement of thermal conductivity. In addition, the average size of Fe_3O_4–GNP/water was 327 nm compared to Fe_3O_4/water at around 60.4 nm. The formation of clustering of GNP sheets with

a higher tendency to stick to each other was concluded to be one of the contributions to the thermal conductivity enhancement of hybrid nanofluid. Batmunkh *et al.* [176] experienced a slight increase in thermal conductivity from 1.5 to 3.2% when mono-TiO_2 and TiO_2–Ag were dispersed in water at 15°C, respectively. However, as the temperature increases, both nanofluids experience a decrease in thermal conductivity ratio. The thermal conductivity of TiO_2/water returns to the value of the water-based fluid at 40°C. The difference in thermal conductivity ratio of this nanofluid is only 0.04%. The conductance contact between nanoparticles has been improved when adding 0.5 wt% of Ag in TiO_2–water. Nevertheless, the thermal conductivity ratio of TiO_2–Ag/water decreases from an increase of 3.2–1.4% when the temperature increases from 15 to 40°C. Since Ag has high thermal conductivity, the interface of TiO_2–Ag hybrid nanoparticles facilitates phonon conduction by reducing the boundary dispersion failure and interfacial resistance between nanoparticles and the fluid.

Figure 5(b) shows the three different nanoparticles dispersed in W:EG 60:40% by volume ratio. The experimental outcome by Chiam *et al.* [95] and Nabil *et al.* [75] on the effect of different types of base fluid was discussed in Section 5.1.1. They also discussed the effect of temperature on thermal conductivity ratio for Al_2O_3 and TiO_2-SiO_2 dispersed in the same base fluid from 30 to 70°C. Like most of the relationship between temperature and thermal conductivity ratio for water-based fluid, the linear increase in thermal conductivity ratio was also achieved for W:EG 60:40%-based fluid with respect to temperature. The thermal conductivity ratio for the same concentration of 1 wt% increases by 4.6 and 5.6% at the temperature 30°C and increases to 7.8 and 9.4% as the temperature increases to 70°C for Chiam *et al.* [95] and Nabil *et al.* [75], respectively. For the same concentration and type of nanofluid as Chiam *et al.* [95], Sundar *et al.* [151] dispersed a slightly bigger size of Al_2O_3 nanoparticles, and the thermal conductivity ratio is higher than Chiam *et al.* [95]. The thermal conductivity ratio is 1.13 at 20°C and is increased to 1.28 at 60°C. As temperature increases, nanoparticles are given higher kinetic energy, which induces micro-convection in nanofluids and correlates with improved thermal conductivity. Increased thermal conductivity is also observed due to the substantial Brownian motion of the nanoparticles in the base fluid. High temperatures can adversely affect clustering and reduce the repulsive forces between nanoparticles, resulting in a less stable mixture with low thermal conductivity [80].

6.2.5 Effect of nanoparticle size

Figure 6 shows the effect of nanoparticles' size on the thermal conductivity ratio of nanofluids. The graph is plotted from two references for aqueous Al_2O_3 [169], TiO_2 [169], and ZnO [161]. The result was recorded for the sample at the same temperature of 25°C at the same volume concentration of 1%. It is evident that, as the nanoparticle size increases, the thermal conductivity ratio decreases for all references. Mintsa *et al.* [169] and Kim *et al.* [161] investigated TiO_2 and ZnO at the same particle sizes of 10 and 30 nm, respectively. ZnO thermal conductivity ratio is higher than TiO_2 for the same particle size of 10 nm, with 1.049 for ZnO and 1.032 for TiO_2. For a larger size of particles, the thermal conductivity of ZnO and TiO_2 decreased to 1.032 and 1.027, respectively. Therefore, the change in thermal conductivity ratio on nanoparticles' size is less than 2% as the size increases from 10 to 30 nm. Mintsa *et al.* [169] also investigated Al_2O_3 dispersed in

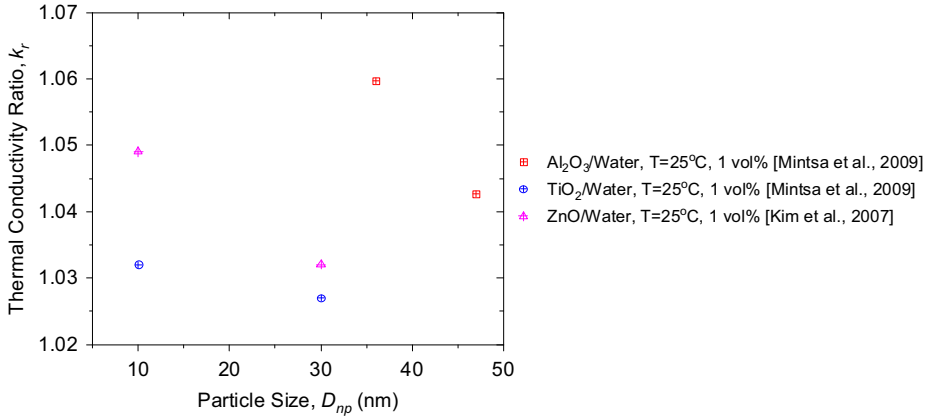

Figure 6: Effect of nanoparticle size on thermal conductivity in a base fluid of water.

water for two different nanoparticle sizes, 36 and 47 nm. The thermal conductivity ratio was 1.06, with Al_2O_3 nanoparticles' size 36 nm reduced by 1.7% as the size of nanoparticles increased to 47 nm. Mintsa *et al.* [169] indicated that for the same volume concentration, a nanofluid with smaller nanoparticles yields an effective thermal conductivity because it has more significant contact with the surface of the fluid and increases the potential of Brownian motion.

Conversely, Timofeeva *et al.* [153] revealed an opposite trend in the particle size's thermal conductivity effect. Four different SiC sizes were tested for their thermal conductivity in water and W:EG 50:50% by volume percentages. The thermal conductivity increases as the average SiC size increases from 16, 28, 66, and 90 nm. Beck *et al.* [170] also previously found the same pattern for aqueous Al_2O_3 nanoparticles. The size of Al_2O_3 was investigated at the wide range of nanoparticle sizes ranging from 8 to 282 nm. For smaller particles sizes up to 50 nm, thermal conductivity has increased as the nanoparticle size increases. Nevertheless, the size of nanoparticles is inadequate for a larger size of nanoparticles as the thermal conductivity is constant. Recent work by Omrani *et al.* [177] has also shown the same pattern for MWCNT. The effect of the size of the MWCNT was determined by measuring the AR. They measured thermal conductivity and dynamic viscosity of MWCNT for six different ARs from the short type, AR ~ 10–40, to the long type, AR ~ 1,250–3,750. The results showed that the thermal conductivity increased linearly as the AR increased for the water-based fluid at the measured temperature.

Besides that, numerous pieces of literature have established the effect of nanoparticle size in a different mode of investigation. Eastman *et al.* [166] reported that for the same volume concentration of 0.5 vol% nanoparticles in EG, thermal conductivity ratio of pure Cu, Cu with an average diameter of less than 10 nm is 10% higher than that of CuO with an average diameter of 35 nm, approximately four times bigger than Cu. Kalantari *et al.* [178], which used citric acid and citrate at various amounts to stabilize aqueous Ag nanoparticles at room temperature, showed that the amount of citric acid in a fluid was influenced by the size of Ag. The size of nano-Ag is decreased as the volume of citric acid increases. In his study, the decrease in the size of Ag contributed to the rise in thermal conductivity. Nevertheless, the thermal conductivity of nano-Ag nanofluids increases by up to 223% compared to the base fluid of water at the same temperature of 50°C. Bouguerra *et al.* [102] indicated that when nanoparticles are monodispersed with the smallest particle size, maximum thermal conductivity and minimum dynamic viscosity were observed. Five different dispersion patterns and alteration of the structure of aqueous Al_2O_3 nanofluids were discovered for a pH range of between 4 and 8 for a volume concentration of between 0.2 and 2% at 25°C. They stressed that the dispersion patterns of nanoparticles in nanofluid could determine the thermal conductivity and dynamic viscosity and their effect on the overall performance of the thermal energy plant.

Recent research by Essajai *et al.* [179] stated that the nanoparticles rod shape of Au nanoparticles provides better thermal conductivity than spherical shape nanoparticles. However, they demonstrated that the rod shape affected the nanofluid diffusion coefficient, which contradicted previous findings by Sarkar *et al.* [135] and Avsec [137]. Alawi *et al.* [142] also analyzed the influence of four different types of metal oxides in various shapes. The thermal conductivity of Al_2O_3, CuO, SiO_2, and ZnO in the shape of blades, bricks cylindrical, platelets, and spherical nanoparticles has been compared. The spherical-shaped Al_2O_3, CuO, and ZnO had the highest thermal conductivity at the highest concentration of 5 vol%. On the other hand, SiO_2 nanofluids obtained the highest thermal conductivity with the same concentration of cylindrical-shaped nanoparticles.

6.3 Dynamic viscosity

Dynamic viscosity is one of the main thermophysical properties for determining continuous fluid deformation with shear stress. It measures the fluid's internal resistance to flow, whether the fluid is deformed by shear stress or by extensional stress. This property plays a significant role in fluid flow and heat transfer, influencing the coefficient of convective heat transfer. Adewumi *et al.* [42] investigated dynamic viscosity to evaluate the necessary pumping power that could, in turn, affect the efficiency of the system. Depending on the reaction of the shear stress to the shear rate, dynamic viscosity may also vary with time and temperature. The rheological properties of nanofluid can be Newtonian and non-Newtonian behaviors depending on the relationship between dynamic viscosity as a function of shear rate and shear stress, as shown in the following equation:

$$\tau = \mu \times \dot{\gamma} \tag{10}$$

where τ is shear stress, μ is viscosity, and $\dot{\gamma}$ is shear rate. For Newtonian fluid behavior, shear stress has a linear relationship to the shear rate. The slope of this relationship remained a constant viscosity. Non-Newtonian behavior,

on the other hand, means that the dynamic viscosity depends on the flow conditions, which are shear rate, temperature, flow geometry, shear time, initial dispersion state, and stability [73]. Non-Newtonian flow models are commonly used in Power law [180]:

$$\tau = K \cdot \dot{\gamma}^n \tag{11}$$

and Herschel-Bulkley;

$$\tau = \tau^{'} + \dot{\gamma}^n \tag{12}$$

where τ is shear stress, K is the flow consistency index, $\dot{\gamma}$ is shear rate, $\tau^{'}$ is yield shear stress, and n is the flow behavior index. Non-Newtonian fluid behavior can be classified as time-independent fluid and time-dependent fluid. The time-independent fluid is independent of the shear duration. It can be divided into three different groups, including shear-thinning, shear-thickening, and visco-plastic fluids. Shear-thinning, also known as pseudoplastic fluids, reduces viscosity by increasing the shear rate. Shear thickening, on the other hand, increases the viscosity as the shear rate increases. Visco-plastic occurs when the yield stress, τ_0 is reached before the fluid starts to flow. For time-dependent fluid, it can be divided into two types of thixotropic and rheopectic fluid. Thixotropic fluid occurs when the apparent viscosity decreases over time at the constant shear rate. On the other hand, the rheopectic fluid displays the reversed behavior when the apparent viscosity increases over time at a constant shear rate.

The dynamic viscosity of nanofluids is influenced by nanoparticle volume concentrations, temperature, nanoparticle size and shape, pH, and surfactants [49]. Hamze *et al.* [181] also provided a complete review of the influences of GE-based nanofluid concentration, temperature, base fluid, shear rate, and surfactant on dynamic viscosity. This review study, on the other hand, will examine and compare the three most investigated factors impacting nanofluid dynamic viscosity.

6.3.1 Effect of concentration

Figure 7 shows the standard dynamic viscosity data as a function of the bulk temperature of the commonly used base fluid for nanofluids investigations and applications. It shows that dynamic viscosity decreases exponentially as temperature increases from 20 to 80°C. The lowest dynamic viscosity of the base fluid is water with 1.0 mPa s at 20°C and drops to 0.3543 mPa s at 80°C [143]. EG's highest dynamic viscosity is 19.486 mPa s at 20°C and decreases to 2.98 mPa s at 80°C [168]. The W:EG mixture at various volume ratios is actively investigated to apply convection heat transfer [95,151]. The dynamic viscosity of the W:EG mixture is increased as more EG is added to the water-based fluid [144]. Dynamic viscosity may change due to the presence of solid nanoparticles through concentrations and may lead to an increase in the pressure drop, thereby affecting the efficiency of energy systems. Low dynamic viscosity is desired to reduce pressure drop, increase fluid velocity, and increase energy efficiency for effective drag reduction or forced convection heat transfer applications.

Thus, Figure 8 shows the relationship between dynamic viscosity ratio *versus* normalized weight or volume concentration for various types of nanoparticles dispersed in water, W:EG 60:40%, and EG. The range of the concentration for presented nanofluids can be referred in Tables 1 and 2. The comparison was made for nanofluid at temperatures between 20 and 30°C without any surfactant. Although the size of nanoparticles and pH value may impact the dynamic viscosity measurement of nanofluids, this effect is ignored in

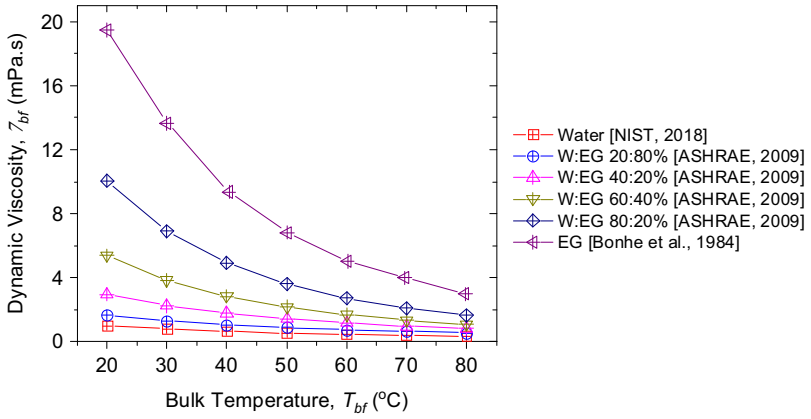

Figure 7: Dynamic viscosity of various types of base fluids.

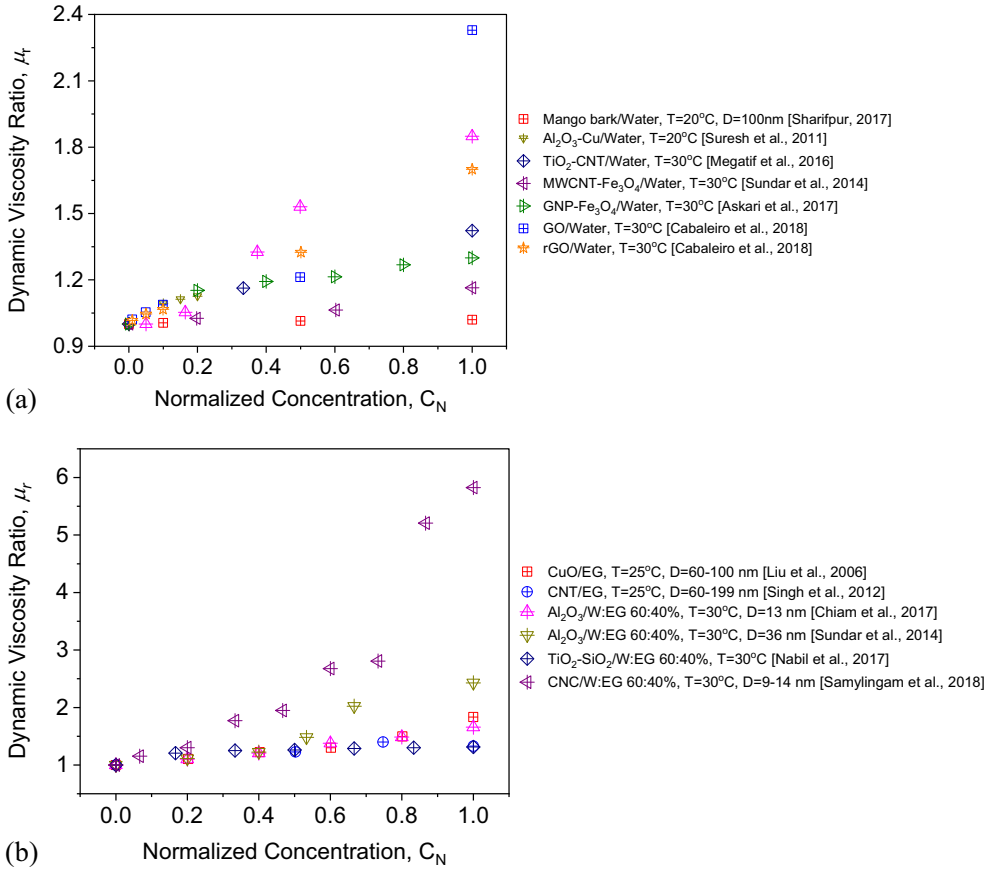

Figure 8: Effect of concentration on dynamic viscosity: (a) water and (b) EG and W:EG 60:40% mixture.

this comparison. The dynamic viscosity ratio is increasing linearly as the normalized concentration increases.

Figure 8(a) shows the lowest dynamic viscosity ratio was gained by mango bark nanofluids. The aqueous mango bark with an average size of 100 nm increases dynamic viscosity by only 2% when nanoparticle concentration has increased to 1 vol% at a constant temperature of 20°C [38]. Barki *et al.* [70] also synthesized the mango bark in the laboratory, and the size of the nanoparticle is 200 nm. This nanoparticle was dispersed at a concentration from 0.1 to 4 vol% in water at the same temperature of 20°C. Comparing the results of Sharifpur *et al.* [38] and Bakri *et al.* [70] at the same concentration of 1 vol%, the dynamic viscosity from Bakri *et al.* [70] significantly decreased by 1% compared to the water-based fluid. Since the dynamic viscosity was reduced with the existence of nanoparticles in the fluid, mango bark might be suitable to be used as a drag reduction agent. However, as the concentration rose to 4 vol%, the dynamic viscosity increased exponentially to 107% relative to the base fluid. On the other hand, the hybrid aqueous GO reached an undesired highest dynamic viscosity by 233%, with a weight concentration of 1 vol%. On the other hand, in Figure 8(b), the lowest dynamic viscosity was achieved by CNT-EG and TiO_2–SiO_2/W:EG 60:40% with a respective concentration of 0.4 wt% and 3 vol%. The result of hybrid Al_2O_3 and TiO_2 is consistent with the previous work of mono Al_2O_3 and TiO_2 in W:EG 80:20% by Yiamsawas *et al.* [182]. Mono Al_2O_3 and TiO_2 nanofluid were investigated at the volume concentration range between 1 and 4% and temperature range of 15–60°C. The result has shown that Al_2O_3 nanofluid has a higher dynamic viscosity than TiO_2 nanofluid. They clarified that the result was obtained because Al_2O_3 has a larger particle size than TiO_2. The effect of particle size on dynamic viscosity ratio will be discussed in Section 6.3.3.

To obtain a more distinct difference in dynamic viscosity ratio between nanofluids, the dynamic viscosity ratio at the same concentration is shown in Table 3. Water-based nanofluids for 0.1 and 1 wt% and EG or W:EG 60:40%-based nanofluids for 0.1 and 1 vol% are shown in Table 3(a) and (b), respectively. The comparison was made for the sample temperature between 20 and 30°C. It shows that in water-based fluid, mango bark

Table 3: Dynamic viscosity ratio for nanofluids

Refs.	Nanoparticles	Dynamic viscosity ratio (0.1 wt%)	Dynamic viscosity ratio (1 wt%)
(a) Water-based fluid			
[70]	Mango bark	0.943 (0.125 wt%)	2.066
[38]	Mango bark	1.005	1.02
[91]	GNP–Fe_3O_4	1.026	—
[109]	TiO_2–CNT	1.094	—
[158]	GNP–Ag	1.3	—
(b) EG or W:EG 60:40%-based fluid			
[164]	CuO	—	1.104
[75]	TiO_2:SiO_2	—	1.252
[95]	Al_2O_3	—	1.658
[151]	Al_2O_3	—	2.023
[16]	CNC	1.154	2.678 (0.9 vol%)

produced in a laboratory by Barki *et al.* [70] with a concentration of 0.125 wt% reduces the dynamic viscosity by 5.7%. This result indicates that this organic-based nanofluid has the potential to be used as a drag reduction additive. The drag reduction phenomenon was initiated by Forrest back in 1931 by dispersing wood pulp in the pipe flow. The dispersion of a minimal amount of pulp or particles called a drag reduction additive reduces the viscous friction and pressure drop, thereby minimizing power consumption [183]. Consequently, for the same Reynolds number in the pipe flow, the reduction of dynamic viscosity will help to accelerate the flow velocity and increase power consumption efficiency. Nevertheless, as the concentration of aqueous mango bark increased to 1 wt%, the dynamic viscosity increased exponentially by 106.6%, and a drag reduction additive is no longer effective. Mango bark produced by Sharifpur *et al.* [38] may be used as a drag reduction additive as the dynamic viscosity ratio for both nanoparticles almost constant for 0.1–1 wt%. On the other hand, other nanoparticles show an increase in the dynamic viscosity ratio at all concentrations. Samylingam *et al.* [16] obtained the highest dynamic viscosity compared to other nanofluids with an exponential rise of up to 167.8% at 1 vol%. As the concentration increased to 1.5 vol%, the dynamic viscosity ratio increased to 5.826. Contradictory, they wanted a low viscous fluid to pump the fluid into the cutting interphase of the lathe machine operation. This nanofluid was investigated to improve the cutting speed, cutting depth, and feed rate of the lathe cutting machine, thus improving the heat transfer and tool life.

Askari *et al.* [91] said that by increasing the concentration of GE–Fe_3O_4 nanoparticles in water, the attractive force becomes greater than the repulsive force resulting in nanoparticles sticking together, leading to an increase in the dynamic viscosity of the nanofluid. Chiam *et al.* [95] dispersed Al_2O_3 nanoparticles in three different volume ratio mixture of W:EG and claimed an increase in dynamic viscosity as the concentration increased because more nanoparticles are added in the respective base fluid that causes an increase in friction and flow resistance of nanofluids. They added that the nanoparticles dispersed in the higher volume ratio of EG have higher dynamic viscosity. This inference is appropriate because, based on the standard data from ASHRAE, the dynamic viscosity of the higher volume ratio of EG has a higher dynamic viscosity than that of the higher volume ratio of water. Nevertheless, a dynamic viscosity percentage increase should be independent of the base fluid's dynamic viscosity, but only the nanofluid's concentration [153]. The observed anomalies could be correlated with the difference between the structure and thickness of the interfacial layer around the nanoparticles in the various base fluid, which affect the effective nanofluid concentration and, ultimately, the dynamic viscosity of nanofluids.

Suresh *et al.* [171] stated that the volume concentration from 0.001 to 0.02% of aqueous Al_2O_3–Cu did not change the Newtonian behavior of water. The Newtonian behavior was preserved at all concentrations as the shear rate increased from 0 to 750 s^{-1}. The dynamic viscosity of aqueous hybrid Al_2O_3–Cu nanofluid did not vary significantly from that of aqueous mono Al_2O_3 nanofluid at a lower concentration. However, the disparity is noticeable at higher volume concentrations. The rationale is that, as the nanofluids concentration increased, the clustering and adsorption increase the hydrodynamic diameter of nanoparticles, leading to an increase in the dynamic viscosity ratio. Nabil *et al.* [75] observed a Newtonian behavior in TiO_2–SiO_2/W:EG 60:40% nanofluids when a range of shear rate was applied from 25 to 180 s^{-1}. Newtonian behavior was observed before 3 vol% and temperature of between 30 and 50°C. Similar behavior was observed in Sundar *et al.* [151] for Al_2O_3/W:EG 60:40% for a concentration range of 0.3–1.5 vol% and a temperature range of 20–60°C. Yu *et al.* [184] also observed Newtonian fluid for ZnO/EG at a concentration below 2 vol% from 20 to 60°C since the viscosity is independent of shear rate from 20 to 100 s^{-1}. Nevertheless, a shear-thinning behavior was observed at a higher concentration of 3 vol% at a temperature below 40°C. As the concentration increases to 5 vol%, the shear-thinning was observed at all temperature under investigation from 20 to 60°C. The explanation for the shear-thinning was observed at this condition because the effective volume fraction of aggregates was much higher than the actual solid volume fraction. Chavan *et al.* [106] found the same pattern for Al_2O_3/water and SiO_2/EG at a shear rate of 0.1–500 s^{-1} at 30°C. Both

nanofluids are Newtonian with a concentration of less than 1 vol%, and the dynamic viscosity slope of Al_2O_3/water is steep than SiO_2/EG. These findings show that the dynamic viscosity of Al_2O_3/water is higher than that of SiO_2/EG. Shear-thinning was observed for concentrations above 4 vol%.

On the other hand, Garg *et al.* [180] studied the influence of ultrasonication on the dynamic viscosity of aqueous MWCNT at 1 wt% mixed with GA at 0.25 wt% nanofluid at 15 and 30°C. Ultrasonication was conducted for 20–80 min, with an interval of 20 min. They have shown that this nanofluid exhibits a shear-thinning or pseudoplastic type of non-Newtonian behavior without the presence of surfactant when a shear rate of up to 60 s^{-1} at 15°C has been applied at all ultrasonication time. The shear-thinning effect was characterized by the potential de-agglomeration or realignment of the bundled nanotubes in the direction of the shearing force, resulting in less viscous drag. As the ultrasonication time increases, the nanotube spread, leading to the less pronounced shear-thinning behavior of the nanotube due to the shorter nanotube sizes.

6.3.2 Effect of bulk temperature

Figure 9(a) and (b) shows the effect of bulk temperature on the dynamic viscosity ratios of water, EG, and W:EG 60:40% by volume ratio nanofluids. The comparison is made for hybrid nanofluids with concentrations of less than 0.1 wt% or 1 vol%. Ten mono and hybrid nanofluids were plotted, and the trends differed for all nanofluids. At the respective temperature ranges, all nanofluids exhibit a greater dynamic viscosity ratio than the base fluid, except for mango bark at concentrations less than 0.5 vol%. When compared to the base fluid, all synthetic nanofluids increased dynamic viscosity by at least 5%. Fe_3O_4/water, GNP–Fe_3O_4/water, and CNT–TiO_2/water exhibit substantially similar dynamic viscosity ratios at all temperatures with the same concentration and the lowest increment when compared to other synthetic nanofluids. Al_2O_3/W:EG 60:40% from Chiam *et al.* [95] has a constant decrease, whereas Al_2O_3/W:EG 60:40% from Sundar *et al.* [151] fluctuates and exhibits the most significant rise in dynamic viscosity ratio as temperature increases. GNP–Ag/water and GQD/W:EG 60:40% show a consistent increase, while other nanofluids fluctuate as the temperature rises. According to Yarmand *et al.* [158], Barki *et al.* [70], Adewumi *et al.* [42], Aberoumand *et al.* [185], and Nguyen *et al.* [186], the increases in dynamic viscosity of any nanofluid can be attributed to the weakening of inter-particle and inter-molecular adhesive forces caused by an increase in heat convection between nanoparticles.

The dynamic viscosity of aqueous mango bark is almost identical to the base fluid relative to other nanofluids presented [113]. The dynamic viscosity ratio of aqueous mango bark decreases at low temperatures and concentrations. At the same volume concentration of 0.1%, the dynamic viscosity ratio of aqueous mango bark is lower than the base fluid. The lowest drop in dynamic viscosity ratio was reached at 60°C with a decrement of 21.8%. As the volume concentration increased to 0.5%, the dynamic viscosity increased by 3.2% at 10°C compared to the base fluid. As the temperature increases to 15°C, the dynamic viscosity decreases by 5.9% below the base fluid. As the temperature rises to 35°C, this value is retained below 5% of the base fluid. The dynamic viscosity ratio increased as the concentration rose to 1 vol%. The value increases to 8% at 10°C and decreases slightly below the dynamic viscosity of the base fluid with a tolerance of 1% to 35°C. These findings show an exciting feature of drag reduction for organic-based nanofluids at lower concentrations and temperatures as lower dynamic viscosity of nanofluids reduces the pumping power needed to drive the flow. The dynamic viscosity ratio then increases significantly as the temperature increases to a maximum value of 12.5% at 60°C. After which, the dynamic viscosity ratio of aqueous mango barks appeared to increase with temperature and concentrations dramatically. Nonetheless, the dynamic viscosity ratio of aqueous banana stem increased immediately following the 0.3 vol% nanoparticle concentration dispersed at 20°C [187]. With this concentration, the dynamic viscosity of nanofluid increased by 6%. The dynamic viscosity ratio increases to 1.14 as the temperature increases to 60°C. The maximum dynamic viscosity ratio of banana stem is 1.22, with a concentration of 1.5 vol% at 20°C.

6.3.3 Effect of nanoparticle size

The dynamic viscosity can change up to 40% by varying the size of particles [188]. Since the suggestion made by Forrest and Grierson on the effect of particle shape, size, and ARs may have an impact on the thermophysical properties of nanofluid, especially dynamic viscosity for drag reduction, several studies have been conducted on this relationship [189–191]. Figure 10 provides examples of the effect of the size of Al_2O_3 in EG on the dynamic viscosity ratio at 25°C by three different references. The effect of the size of Al_2O_3 is only noticeable at higher concentrations. The distinction was therefore provided

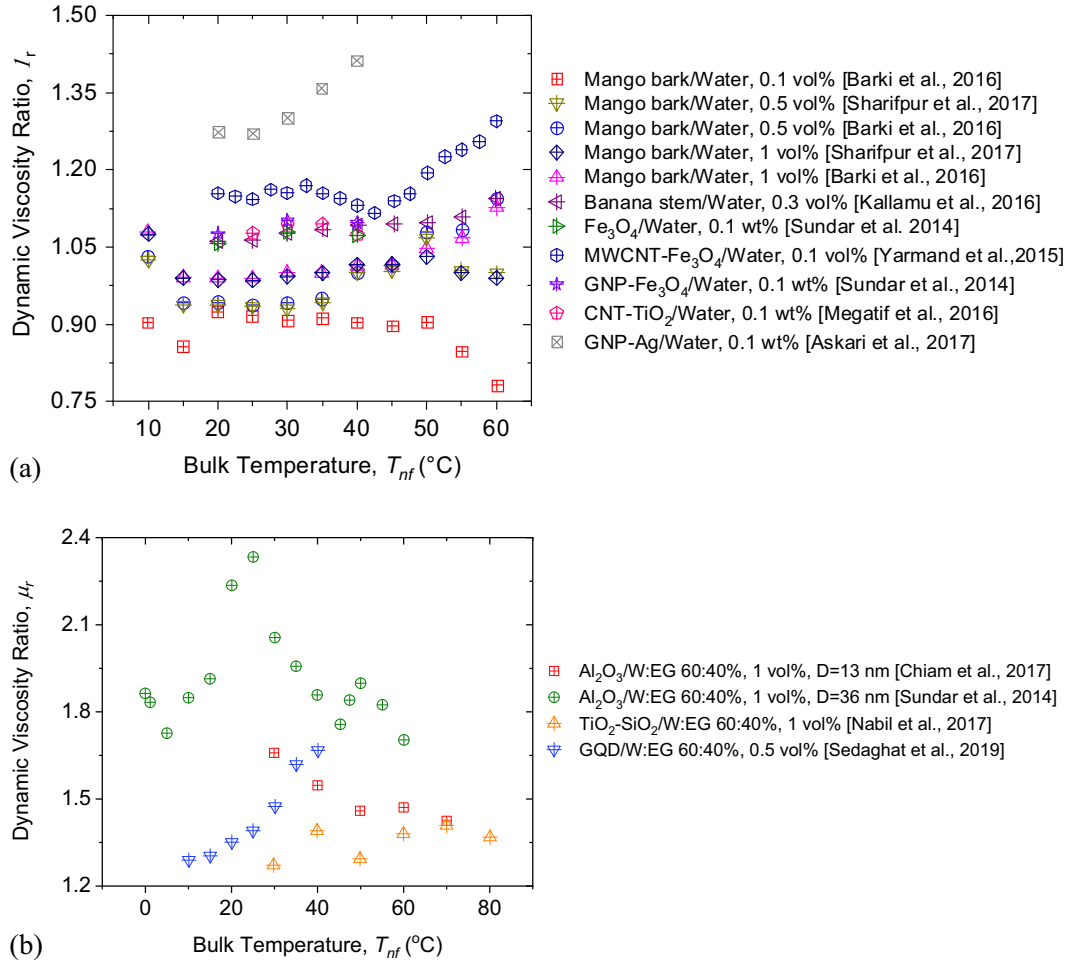

Figure 9: Effect of bulk temperature on normalized dynamic viscosity: (a) water and (b) W:EG 60:40%.

with a volume concentration of 5% for all samples. The dynamic viscosity ratio from Kwek *et al.* [192] and the other two references are contradictory. The dynamic viscosity ratio of the sample from Kwek *et al.* [192] decreased, and the dynamic viscosity ratio of the sample from Adio *et al.* [193] and Selvam *et al.* [100] increased marginally as the particle size increased. The dynamic viscosity ratio decreases by 47.8% as particle size increases from 10 to 80 nm as the particle size increases for the sample from Kwek *et al.* [192]. Timofeeva *et al.* [153] agreed with Kwek *et al.* [192] for SiC/water and SiC/W:EG 50:50% of the same concentration, temperature, and pH value. The dynamic viscosity ratio is more profound for smaller particle size than for larger ones. Adio *et al.* [193] described that at the same volume concentration, the smaller size of nanoparticles provides a higher quantity of nanoparticles in the same volume concentration of nanofluid. The interaction between smaller nanoparticles will increase the Brownian velocity and the electro-viscous effect between them, contributing to the increment in viscosity. Therefore, the dynamic viscosity of nanofluid is higher with smaller nanoparticles. When the particle size is sufficiently small, starting from a specific critical size, it interacts actively with each other. At the same time, the fluid near the nanoparticles is formed to alter the rheological behavior, including the dynamic viscosity of the nanofluid [194].

On the other hand, Omrani *et al.* [177] demonstrated the decrement of dynamic viscosity as the CNT AR at the temperature of 25°C with a volume fraction of 0.05 vol%. The higher AR is more desirable as the dynamic viscosity ratio is the lowest at the highest AR at 2,500 compared to the lowest AR at 100. Alawi *et al.* [142] reveal that platelet-shaped nanoparticles for four different types of metal oxide have significantly reduced in dynamic viscosity compared to other shapes. However, he did not explain the rheological mechanism of the nanoparticles shape effect.

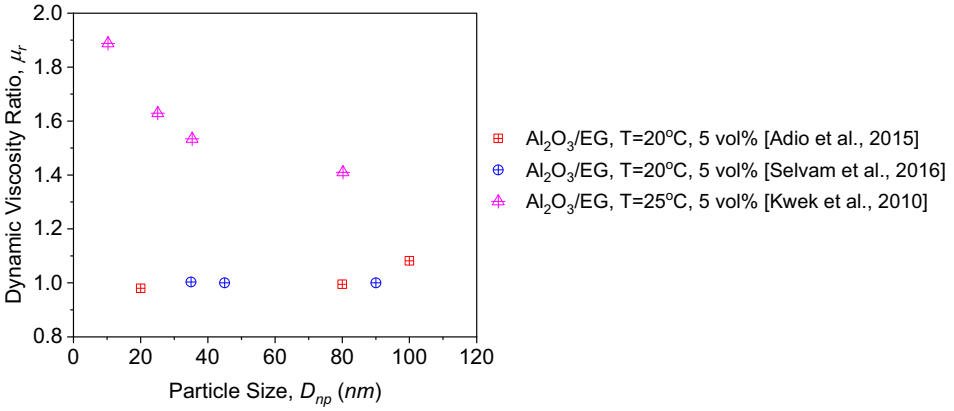

Figure 10: Effect of nanoparticle size in EG on dynamic viscosity ratio.

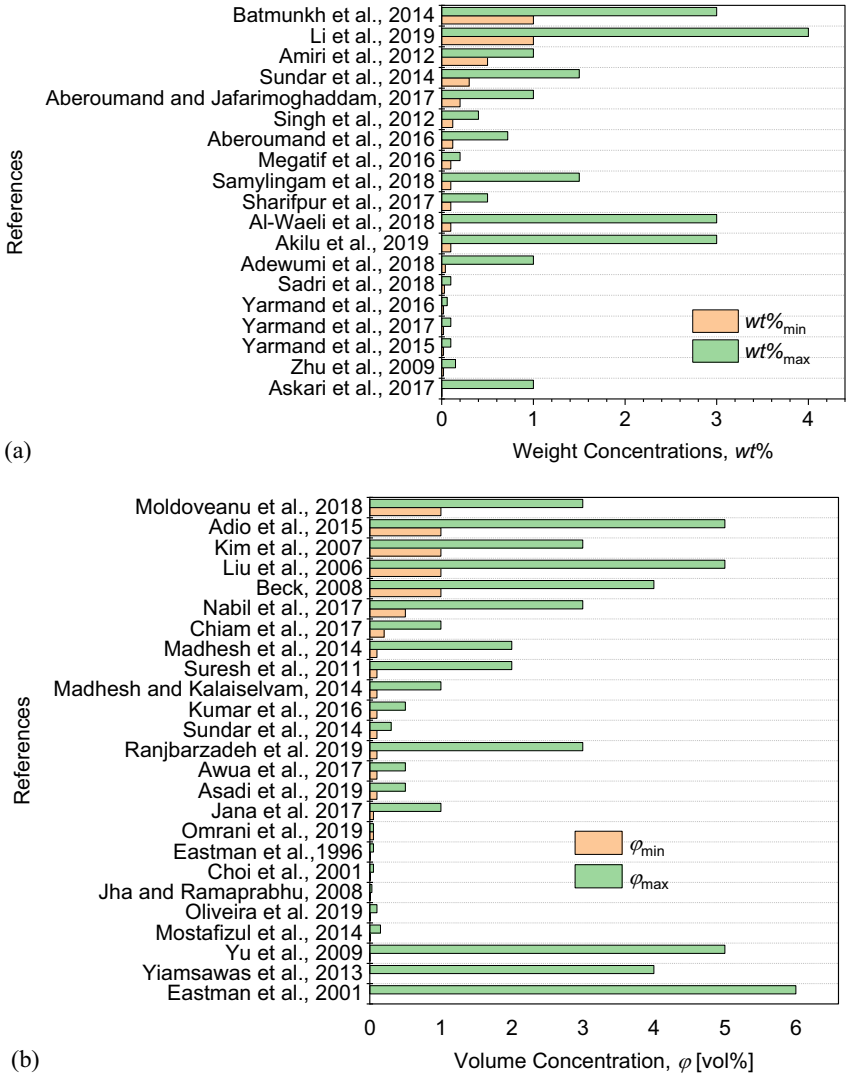

Figure 11: Range of weight and volume concentrations: (a) weight concentrations and (b) volume concentrations.

7 Author's observation

Figure 11 displays the distribution of minimum and maximum weight and volume concentrations used to investigate nanofluids. These data were extracted from Tables 1 and 2. From the observation, all researchers prefer to begin the nanofluid investigation with a minimum concentration of less than 1 wt% or 1 vol%. Out of 35 researchers in Figure 11(a) and (b), 48.6% of researchers started their investigations at concentrations below 0.1%. On the other hand, 70% of them examine the effect of nanofluids concentrations up to a maximum of more than 1% by weight or volume. However, the authors did not offer any explanation for selecting the spectrum of the concentration under their investigation.

A small concentration of less than 1% by weight or volume primarily aims to reduce unwanted increases in dynamic viscosity while maintaining optimal thermal conductivity. In contrast, to maximize the effect of nanoparticle dispersion in the base fluid to boost heat transfer, a greater range of nanofluid concentrations were chosen for the investigation to maximize the enhancement in thermal conductivity, even if the dynamic viscosity is indeed multiplied. Nonetheless, since the trend of thermal conductivity and dynamic viscosity for nanofluid concentration is monotonic, determining the optimum concentration of nanofluids is practically impossible without establishing a limit or constraint on the desired output. Talari *et al.* [195] set a temperature drop of up to 15°C of a hot fluid in a corrugated plate type heat exchanger utilizing water-based Al_2O_3 as a coolant to discover the optimum nanoparticle concentrations. Simultaneously, the minimum critical flow rate was determined to estimate the maximum hydraulic power adequate for the configured pumping system. Rejvani *et al.* [196] employed a Nondominated Sorting Genetic Algorithm II (NSGA-II) to determine the optimal SiO_2/water concentration for maximum thermal conductivity and minimum viscosity. The algorithm's output is the ratio of dynamic

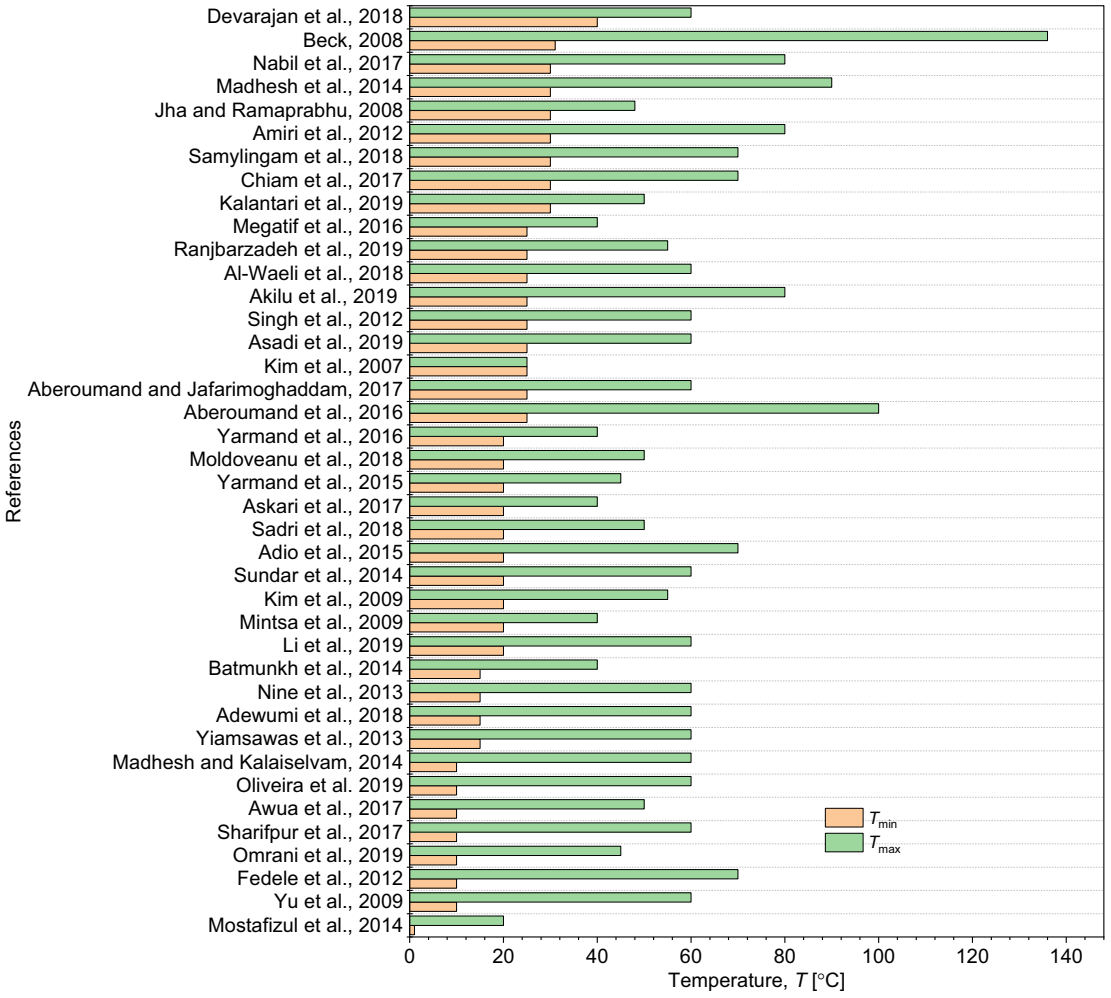

Figure 12: Range of temperatures.

viscosity enhancement to dynamic viscosity enhancement, and the Mouromtseff number was suggested for further application. Esfe *et al.* [197] employed a modified NSGA-II in conjunction with multi-layer perceptron neural network modeling to determine the concentration of Al_2O_3/W:EG 20:80%. The ideal point is then shown as the Pareto Front.

In addition, as shown in Figure 12, 44% out of the 41 investigators have begun the investigation above 25°C, and 98% of them limit the study below 100°C. The temperature of nanofluids may increase when used as a working fluid for mechanical machines such as heat exchangers, pumps, and turbines. As a result, expanding the temperature spectrum above 100°C for water-based fluid alters the nanofluid's properties to boiling heat transfer investigations. Various synthetic- and organic-based nanoparticles have been used in nanofluids' investigations. Even then, the reason for selecting specific types of nanoparticles has rarely been clarified in the debate. At the same time, synthetic-based fluids such as Cu, Ag, Al_2O_3, CuO, TiO_2, Fe_3O_4, and various carbon-based nanoparticles have been significantly investigated for thermal conductivity and dynamic viscosity compared to organic nanofluids. Therefore, further detailed investigation of organic-based nanofluids is needed. Even in existing studies on organic-based nanofluids, few organic materials in mini or milli-sized particles suspension such as Kenaf, coconut fiber, chitosan, and clove buds have been dispersed in synthetic-based nanofluid to enhance heat transfer. Extensive work is required to find the optimum thermal conductivity and dynamic viscosity for the same materials in nano-sized and new investigations of any high conductive organic nanoparticles. It is known from the literature that the mixture of two or more types of nanoparticles for nanofluid provides excellent results in terms of thermal conductivity. Nonetheless, almost all studies have shown that the mixture is made up of two synthetic-based nanoparticles. Further analysis of mixture organic- and synthetic-based nanoparticles and their drag reduction and heat transfer enhancement is needed. The aim is to achieve the highest thermal conductivity and the lowest effect on the dynamic viscosity of nanofluid in any fluid mechanics and heat transfer applications.

8 Conclusion

Mono and hybrid synthetic- and organic-based nanoparticles dispersed in a base fluid of water, EG, and a mixture of W:EG 60:40% were selected to investigate the effects of nanofluids concentrations, bulk temperature, and the size of nanoparticles. The data comparison of these nanofluids found that the thermal conductivity and dynamic viscosity ratio increased as the normalized concentration of all synthetic-based nanofluids increased. The thermal conductivity of the majority of nanofluids increased by 20% by dispersing mono or hybrid synthetic-based nanoparticles. Thermal conductivity ratio of nanofluids improved by less than 10% by adding carbon-based nanoparticles to metal- or metal oxide-based nanofluid. When the bulk temperature rose to 90°C, the thermal conductivity ratio increased, and the dynamic viscosity ratio is scattered. The thermal conductivity ratio decreased by less than 2% as the particle size increased by 20 nm, and mainly the dynamic viscosity ratio was reduced as the particle size increased. An extensive study of organic-based nanoparticles with high thermal conductivity should be investigated as it may increase the thermal conductivity ratio with minimal impact on the dynamic viscosity of nanofluids.

Funding information: The authors would like to thank the Center of Excellence for Advanced Research in Fluid Flow (CARIFF) for providing financial support under Universiti Malaysia Pahang (UMP) Internal Fundamental Research Grant (University reference RDU190385) and UMP for laboratory facilities.

Author contributions: All authors have accepted responsibility for the entire content of this manuscript and approved its submission.

Conflict of interest: The authors state no conflict of interest.

References

[1] Serrano E, Rus G, Garcia-Martinez J. Nanotechnology for sustainable energy. Renew Sust Energ Rev. 2009;13:2373–84.
[2] Yu W, Xie H. A review on nanofluids: preparation, stability mechanisms, and application. J Nanomater. 2012;17.
[3] Choi SUS, Zhang ZG, Yu W, Lockwood FE, Grulke EA. Anomalous thermal conductivity enhancement in nanotube suspensions. Appl Phys Lett. 2001;79(14):2252–4.
[4] Xuan Y, Li Q. Heat transfer enhancement of nanofluids. Int J Heat Fluid Flow. 2000;21:58–64.
[5] Yoo DH, Hong KS, Yang HS. Study of thermal conductivity of nanofluids for the application of heat transfer fluids. Thermochim Acta. 2007;455:66–9.
[6] Saidur R, Leong KY, Mohammed HA. A review on applications and challenges of nanofluids. Renew Sustain Energy Rev. 2011;15(3):1646–68.

[7] Azmi WH, Sharma KV, Mamat R, Najafi G, Mohamad MS. The enhancement of effective thermal conductivity and effective dynamic viscosity on nanofluids-A review. Renew Sustain Energ Rev. 2016;53:1046–58.
[8] Devendiran DK, Amirtham VA. A review on preparation, characterization, properties and applications of nanofluids. Renew Sustain Energy Rev. 2016;60:21–40.
[9] Sahin AZ, Uddin MA, Yilbas BS, Al-Sharafi A. Performance enhancement of solar energy using nanofluids: an update review. Renew Energy. 2020;145:1126–48.
[10] Zayed ME, Zhao J, Du Y, Kabeel AE, Shalaby SM. Factors affecting the thermal performance of the plate solar collector using nanofluids: a review. Sol Energ. 2019;182:382–96.
[11] Wahab A, Hassan A, Qasim MA, Ali HM, Babar H, Sajid MU. Solar energy systems - Potential of nanofluids. J Mol Liq. 2019;289:111049.
[12] Pordanjani AH, Aghakhani S, Afrand M, Mahmoudi B, Mahian O, Wongwises S. An updated review on application of nanofluids in heat exchangers for saving energy. Energy Convers Manag. 2019;198:111886.
[13] Sajid MU, Ali HM. Recent advances in application of nanofluids in heat transfer devices: a critical review. Renew Sustain Energy Rev. 2019;103:556–92.
[14] Kumar A, Subudhi S. Preparation, characterization and heat transfer analysis of nanofluids used for engine cooling. Appl Therm Eng. 2019;160:114092.
[15] Rahman SS, Ashraf MZI, Amin AKMN, Bashar MS, Ashik MFK, Kamruzzaman M. Tuning nanofluids for improved lubrication performance in turning biomedical grade titanium alloy. J Clean Prod. 2019;206:180–96.
[16] Samylingam L, Anamalai K, Kadirgama K, Samykano M, Ramasamy D, Noor MM, et al. Thermal analysis of cellulose nanocrystal-ethylene glycol nanofluid coolant. Int J Heat Mass Transf. 2018;127:9.
[17] Sidik NAC, Samion S, Ghaderian J, Yazid MNAWM. Recent progress on the application of nanofluids in minimum quantity lubrication machining: a review. Int J Heat Mass Transf. 2017;108:79–89.
[18] Sun C, Boluk Y. Rheological behavior and particle suspension capability of guar gum: sodium tetraborate decahydrate gels containing cellulose nanofibrils. Cellulose. 2016;23:10.
[19] Hassanean MH, Awad ME, Marwan H, Bhran AA, Kaoud M. Studying the rheological proprties and the influence of drag reduction on a waxy crude oil in pipeline flow. Egypt J Pet. 2016;25:39–44.
[20] Watson L. Development of a switchable, tunable surfactant drag reduction solution for application in recirculating heat transport systems. [Bachelor dissertation] The Ohio State University; 2018.
[21] Yunda E, Godymchuk A. Dissolution of zinc nanoparticles in pulmonary fluid: 7th International Forum on Strategic Technology (IFOST). Russia: IEEE; 2002.
[22] Murshed SMS, Estellé P. A state of the art review on viscosity of nanofluids. Renew Sustain Energy Rev. 2016;76:1134–52.
[23] Al Shdaifat MY, Zulkifli R, Sopian K, Salih AA. Thermal and hydraulic performance of CuO/water nanofluids: a review. Micromachines. 2020;11(4):1–19.
[24] Eshgarf H, Kalbasi R, Maleki A, Shadloo MS, Karimipour A. A review on the properties, preparation, models and stability of hybrid nanofluids to optimize energy consumption. J Therm Anal Calorim. 2021;144(5):1959–83.
[25] Zainon SNM, Azmi WH. Recent progress on stability and thermo-physical properties of mono and hybrid towards green nanofluids. Micromachines. 2021;12:176.
[26] Pavia M, Alajami K, Estellé P, Vigolo B. A critical review on thermal conductivity enhancement of graphene-based nanofluids. Adv Colloid Interface Sci. 2021;294:102452
[27] Suganthi KS, Rajan KS. Metal oxide nanofluids: review of formulation, thermo-physical properties, mechanisms, and heat transfer performance. Renew Sustain Energy Rev. 2017;76:226–55.
[28] Gupta M, Singh V, Kumar S, Kumar S, Dilbaghi N, Said Z. Up to date review on the synthesis and thermophysical properties of hybrid nanofluids. J Clean Prod. 2018;190:169–92.
[29] Eastman JA, Choi US, Li S, Thompson LJ, Lee S. Enhanced thermal conductivity through the development of nanofluids. Mater Res Soc Symp Proc. 1996;457:3–11.
[30] Zhai W, Srikanth N, Kong LB, Zhou K. Carbon nanomaterials in tribology. Carbon. 2017;119:150–71.
[31] Bhattacharya M. Polymer nanocomposites - a comparison between carbon nanotubes, graphene, and clay as nanofillers. Materials. 2016;9(262):35.
[32] Jiang H, Zhang Q, Shi L. Effective thermal conductivity of carbon nanotube-based nanofluid. J Taiwan Inst Chem Eng. 2015;55:76–81.
[33] Park J, Yan M. Covalent functionalization of graphene with reactive intermediates. Acc Chem Res. 2013;46(1):181–9.
[34] Hamze S, Berrada N, Cabaleiro D, Desforges A, Ghanbaja J, Gleize J, et al. Few-layer graphene-based nanofluids with enhanced thermal conductivity. Nanomaterials. 2020;10(7):1–21.
[35] Hamze S, Cabaleiro D, Maré T, Vigolo B, Estellé P. Shear flow behavior and dynamic viscosity of few-layer graphene nanofluids based on propylene glycol-water mixture. J Mol Liq. 2020;316:113875.
[36] Sundar LS, Hortiguela MJ, Singh MK, Sousa ACM. Thermal conductivity and viscosity of water based nanodiamond (ND) nanofluids: an experimental study. Int Commun Heat Mass Transf. 2016;76:245–55.
[37] Sadri R, Hosseini M, Kazi SN, Bagheri S, Abdelrazek AH, et al. A facile, bio-based, novel approach for synthesis of covalently functionalized graphene nanoplatelet nano-coolants toward improved thermo-physical and heat transfer properties. J Colloid Interface Sci. 2018;509:140–52.
[38] Sharifpur M, Solomon AB, Meyer JP, Ibrahim JS, Immanuel B. Thermal conductivity and viscosity of mango bark/water nanofluids. 13th International Conference on Mechanics and Thermodynamics. Portoroz, Slovenia; 2017.
[39] Farhanian D, Dion CAD, Raphael W, De Crescenzo G, Tavares JR. Combined extraction and functionalization of low-cost nanoparticles from municipal solid waste fly ash through PICVD. J Env Chem Eng. 2014;2:2242–51.
[40] Awua J, Ibrahim S, Kwaghger A. Investigation of thermal conductivity of palm kernel fibre nanofluid using de-ionized water and ethylene glycol mixed at ration of 50:50 and 60:40. Int J Eng Trends Technol. 2017;49:47–53.
[41] Shirazi SFS, Gharehkhani S, Yarmand H, Badarudin A, Metselaar HSC, Kazi SN. Nitrogen doped activated carbon/graphene with high nitrogen level: green synthesis and

thermo-electrical properties of its nanofluid. Mater Lett. 2015;152:192–95.
[42] Adewumi GA, Inambao F, Sharifpur M, Meyer JP. Investigation of the viscosity and stability of green nanofluids from coconut fibre carbon nanoparticles: effect of temperature and mass fraction. Int J Appl Eng Res. 2018;13(10):7.
[43] Gharehkhani S, Shirazi SFS, Yarmand H, Montazer E, Kazi SN, Ibrahim R, et al. The effect of nanocrystalline cellulose on flow properties of fiber crop aqueous suspension. Carbohydr Polym. 2018;184:376–82.
[44] Bari HAA, Letchmanan K, Yunus RM. Drag reduction characteristics using aloe vera natural mucilage: an experimental study. J Appl Sci. 2011;11(6):1039–43.
[45] Panithasan MS, Gopalakichenin D, Veeraraagavan S. Impact of rice husk nanoparticle on the performance and emission aspect of a diesel engine running on blends on pine oil-diesel. Env Sci Pollut Res. 2019;26:282–91.
[46] Vinukumar K, Azhagurajan A, Vettivel SC, Vedaraman N. Rice husk as nanoadditive in diesel-bio-diesel fuel blends used in diesel engine. J Therm Anal Calorim. 2018;131:1333–43.
[47] Karthik S, Suriyaprabha R, Balu KS, Manivasakan P, Rajendran V. Influence of ball milling on the particle size and antimicrobial properties of Tridax procumbens leaf nanoparticles. IET Nanobiotechnol. 2017;11(1):12–7.
[48] Subramani K, Shanmugam BK, Rangaraj S, Palanisamy M, Periasamy P, Venkatachalam R. Screening the UV-blocking and antimicrobial properties of herbal nanoparticles prepared from Aloe vera leaves for textile applications. IET Nanobiotechnol. 2018;12(4):459–65.
[49] Munyalo JM, Zhang X. Particle size effect on thermophysical properties of nanofluid and nanofluid based phase change materials: a review. J Mol Liq. 2018;265:77–87.
[50] Rajput N. Methods of preparation of nanoparticles – A review. Int J Adv Eng. 2015;7(4):1806–11.
[51] Fuskele V, Sarviya RM. Recent developments in nanoparticles synthesis, preparation and stability of nanofluids. Mater Today: Proc. 2017;4(2):4049–60.
[52] Jamkhande PG, Ghule NW, Bamer AH, Kalaskar MG. Metal nanoparticles synthesis: an overview on methods of preparation, advantages and disadvantages, and applications. J Drug Deliv Sci Technol. 2019;53:101174.
[53] Ganvir RB, Walke PV, Kriplani VM. Heat transfer characteristics in nanofluid – A review. Renew Sustain Energy Rev. 2017;75:451–60.
[54] Babu JAR, Kumar KK, Rao SS. State-of-art review on hybrid nanofluids. Renew Sustain Energy Rev. 2017;77:551–65.
[55] Wagener M, Murty BS, Gunther B. Preparation of metal nanosuspensions by high-pressure DC-sputtering on running liquids. Synposium V – Nanophase and Nanocomposite Material ii; 1997. p. 457.
[56] Wagener M, Gunther B. Sputtering on liquids – a versatile process for the production of magnetic suspensions? J Magn Magn Mater. 1999;201:41–4.
[57] Aberoumand S, Jafarimoghaddam A. Experimental study on synthesis, stability, thermal conductivity and viscosity of Cu-engine oil nanofluid. J Taiwan Inst Chem Eng. 2017;71:315–22.
[58] Lo CH, Tsung TT, Chen LC, Su CH, Lin HM. Fabrication of copper oxide nanofluid using submerged arc nanoparticle synthesis system (SANSS). J Nanopart Res. 2005;7:313–20.
[59] Chang H, Chang YC. Fabrication of Al_2O_3 nanoparticles by a plasma arc nanoparticles synthesis system. J Mater Process Technol. 2008;207:193–9.
[60] Niu HL, Chen QW, Lin YS, Jia YS, Zhu HF, Ning M. Hydrothermal formation of magnetic Ni-Cu Alloy nanocrystallites at low temperatures. Nanotechnology. 2004;15(8):1054.
[61] Darr JA, Zhang J, Makwana NM, Weng X. Continuous hydrothermal synthesis of inorganic nanoparticles: applications and future direction. Chem Rev. 2017;117(17):11125–238.
[62] Lee SW, Park SD, Bang IC. Critical heat flux for CuO nanofluid fabricated by pulsed laser ablation differentiating deposition characteristics. Int J Heat Mass Transf. 2012;55:6908–15.
[63] Phuac TX, Soong Y, Chyu MK. Synthesis of Ag-deionized water nanofluids using multi-beam laser ablation in liquid. Opt Lasers Eng. 2007;45(12):1099–106.
[64] Mahbubul IM. Preparation of nanofluid, in preparation, characterization, properties and application of nanofluid. Oxford, United Kingdom: Elsevier; 2019. p. 15–45.
[65] Kumar A, Yadav N, Bhatt M, Mishra NK, Chaudhary P, Singh R. Sol–gel derived nanomaterials and it's applications: a review. Res J Chem Sci. 2015;5(12):98–105.
[66] Aghababazadeh R, Mirhabibi AR, Pourasad J, Brown A, Brydson R, Banijamali S, et al. Economic synthesis of nanocrystalline alumina using an environmentally low-cost binder. Surf Sci. 2007;601:2864–7.
[67] Mishra PK, Sen S, Amin R, Biring S. Effect of annealing on structure, optoelectronic and photoresponsivity properties of sol–gel prepared ZnO nanoparticles. Mater Today: Proc. 2019;17:261–5.
[68] Das PK. A review based on the effect and mechanism of thermal conductivity of normal nanofluids and hybrid nanofluids. J Mol Liq. 2017;240:420–46.
[69] Akoh H, Tsukasaki Y, Yatsuya S, Tasaki A. Magnetic properties of ferromagnetic ultrafine particles prepared by vacuum evaporation on running oil substrate. J Cryst Growth. 1978;45:495–500.
[70] Barki E, Ibrahim JS, Kuhe A, Iortyer HA. Experimental studies of viscosity and stability of mango bark (Mangifera indica) based nanofluid. 2nd African International Conference/ Workshop on Application of Nanotechnology for Energy, Environment, and Health: African Scenario; 2016. Vol. 2. p. 22–33.
[71] Esmaeili E, Rounaghi SA, Gruner W, Eckert J. The preparation of surfactant-free highly dispersed ethylene glycol-based aluminum nitride-carbon nanofluids for heat transfer application. Adv Powder Technol. 2019;30:2032–41.
[72] Haddad Z, Abid C, Oztop HF, Mataoui A. A review on how the researchers prepare their nanofluids. Int J Therm Sci. 2014;76:168–89.
[73] Asadi A, Aberoumand S, Moradikazerouni A, Pourfattah F, Zyla G, Estelle P, et al. Recent advances in preparation methods and thermophysical properties of oil-based nanofluids: a state of the art review. Powder Technol. 2019;352:209–26.
[74] Arshad A, Jabbal M, Yan Y, Reay D. A review on graphene based nanofluids: Preparation, characterization and applications. J Mol Liq. 2019;279:444–84.
[75] Nabil MF, Azmi WH, Hamid KA, Mamat R, Hagos FY. An experimental study on the thermal conductivity and dynamic

viscosity of TiO_2–SiO_2 nanofluids in water: ethylene glycol mixture. Int Commun Heat Mass Transf. 2017;86:181–9.
[76] Sarkar J, Ghosh P, Adil A. A review on hybrid nanofluids: Recent research, development and applications. Renew Sustain Energy Rev. 2015;43:164–77.
[77] Leong KY, Ahmad KZK, Ong HC, Ghazali MJ, Baharum A. Synthesis and thermal conductivity characteristic of hybrid nanofluids – A review. Renew Sustain Energy Rev. 2017;75:868–78.
[78] Nabil MF, Azmi WH, Hamid KA, Zawawi NNM, Priyandoko G, Mamat R. Thermal-physical properties of hybrid nanofluids and hybrid nanolubricants: a comprehensive review on performance. Int Commun Heat Mass Transf. 2017;83:30–9.
[79] Gupta M, Singh V, Kumar S, Kumar S, Dilbaghi N, Said Z. Up to date on the synthesis and thermophysical properties of hybrid nanofluids. J Clean Prod. 2018;190:169–92.
[80] Sajid MU, Ali HM. Thermal conductivity of hybrid nanofluids: A critical review. Int Commun Heat Mass Transf. 2018;126:211–34.
[81] Babar H, Ali HM. Towards hybrid nanofluids: preparation, thermophysical properties, applications, and challengers. J Mol Liq. 2019;281:598–633.
[82] Bogner A, Jouneau PH, Thollet G, Basset D, Gauthier DC. A history of scanning electron microscopy developments: towards 'wet-STEM' imaging. Micron. 2007;38:390–401.
[83] Kumar PS, Pavithra KG, Naushad M. Characterization techniques for nanomaterials. In: Thomas S, Sakho EHM, Kalarikkal N, Oluwafemi SO, Wu J, editors. Nanomaterials for solar cell applications. Amsterdam: Elsevier; 2019. pp. 97–124.
[84] Yarmand H, Gharehkhani S, Shirazi SFS, Amiri A, Montazer E, Arzani HK, et al. Nanofluid based on activated hybrid of biomass carbon/graphene oxide: synthesis, thermo-physical and electrical properties. Int Commun Heat Mass Transf. 2016;72:10–15.
[85] Nijmegen RU. Information on the FESEM (Field-emission Scanning Electron Microscope) [Internet]. Available from https://www.vcbio.science.ru.nl/public/pdf/fesem_info_eng.pdf
[86] Mamat H. Nanofluids: thermal conductivity and application. In: Reference module in materials science and materials engineering. Amsterdam: Elsevier; 2019. pp. 1–9.
[87] Li F, Li L, Zhong G, Zhai Y, Li Z. Effects of ultrasonic time, size of aggregates and temperature on the stability and viscosity of Cu-ethylene glycol (EG) nanofluids. Int Commun Heat Mass Transf. 2019;129:278–86.
[88] Mahbubul IM, Elcioglu AB, Saidur R, Amalina MA. Optimization od ultrasonication period for better dispersion and stability of TiO_2-water nanofluid. Ultrason Sonochem. 2017;37:360–7.
[89] Asadi A, Alarifi IM, Ali V, Nguyen HM. An experimental investigation on the effect of ultrasonication time on stability and thermal conductivity of MWCNT-water nanofluid: finding the optimum ultrasonication time. Ultrason Sonochem. 2019;58:104639.
[90] Khan AI, Arasu AV. A review of influence of nanoparticle synthesis and geometrical parameters on thermophysical properties and stability of nanofluids. Therm Sci Eng Prog. 2019;11:334–64.
[91] Askari S, Koolivand H, Pourkhalil M, Lotfi R, Rashidi A. Investigation of Fe_3O_4/Graphene nanohybrid heat transfer properties: experimental approach. Int Commun Heat Mass Transf. 2017;87:10.
[92] Nine MJ, Munkhbayar B, Rahman MS, Chung H, Jeong H. Highly productive synthesis process of well dispersed Cu_2O and Cu/Cu_2O nanoparticles and its thermal characterization. Mater Chem Phys. 2013;141:636–42.
[93] Zhu D, Li X, Wang N, Wang X, Gao J, Li H. Dispersion behavior and thermal conductivity characteristics of Al_2O_3-H_2O nanofluids. Curr Appl Phys. 2009;9:9.
[94] Yu F, Chen Y, Liang X, Xu J, Lee C, Liang Q, et al. Dispersion stability of thermal nanofluids. Prog Nat Sci: Mater Int. 2017;27:531–42.
[95] Chiam HW, Azmi WH, Usri NA, Mamat R, Adam NM. Thermal conductivity and viscosity of Al_2O_3 nanofluids for different based ratio of water and ethylene glycol mixture. Exp Therm Fluid Sci. 2017;81:420–29.
[96] Hwang Y, Park HS, Lee JK, Jung WH. Thermal conductivity and lubrication characteristics of nanofluids. Curr Appl Phys. 2006;6(S1):e67–71.
[97] Oliveira LRD, Ribeiro SRFL, Reis MHM, Cardoso VL, Filho EPB. Experimental study on the thermal conductivity and viscosity of ethylene glycol-based nanofluid containing diamond-silver hybrid material. Diam Relat Mater. 2019;96:216–30.
[98] Bello SA, Agunsoye JO, Hassan SB. Synthesis of coconut shell nanoparticles via a top-down approach: assessment of milling duration on the particle size and morphologies of coconut shell nanoparticles. Mater Lett. 2015;159:514–9.
[99] Zubir MNM, Badarudin A, Kazi SN, Ming HN, Misran M, Sadeghinezhad E, et al. Experimental investigation on the use of reduced graphene oxide and its hybrid complexes in improving closed conduit turbulent forced convection heat transfer. Exp Therm Fluid Sci. 2015;66:290–303.
[100] Selvam C, Lal DM, Harish S. Thermophysical properties of ethylene glycol-water mixture containing silver nanoparticles. J Mech Sci Technol. 2016;30(3):1271–9.
[101] Sedeh RN, Abdollahi A, Karimipour A. Experimental investigation toward obtaining nanoparticles surficial interaction with basefluid components based on measuring thermal conductivity of nanofluids. Int Commun Heat Mass Transf. 2019;103:72–82.
[102] Bouguerra N, Poncet S, Elkoun S. Dispersion regimes in alumina/water-based nanofluids: simultaneous measurements of thermal conductivity and dynamic viscosity. Int Commun Heat Mass Transf. 2018;92:51–5.
[103] Witharana S, Palabiyik I, Musina Z, Ding Y. Stability of glycol nanofluids – The theory and experiment. Powder Technol. 2013;239:72–7.
[104] Sezer N, Atieh MA, Koc M. A comprehensive review on synthesis, stability, thermophysical properties, and characterization of nanofluids. Powder Technol. 2019;344:404–31.
[105] Okonkwo EC, Wole-Osho I, Kavaz D, Abid M. Comparison of experimental and theoretical methods of obtaining the thermal properties of alumina/iron mono and hybrid nanofluids. J Mol Liq. 2019;292:111377.
[106] Chavan D, Pise DA. Experimental investigation of effective viscosity and density of nanofluids. Mater Today: Proc. 2019;16:504–15.

[107] Wen D, Ding Y. Experimental investigation into the pool boiling heat transfer of aqueous based Y-alumina nanofluids. J Nanopart Res. 2005;7(2):265–74.
[108] Zyla G, Vallejo JP, Fal J, Lugo L. Nanodiamond-ethylene glycol nanofluids: experimental investigation of fundamental physical properties. Int Commun Heat Mass Transf. 2018;121:1201–13.
[109] Megatif L, Ghozatloo A, Arimi A, Shariati-Niasar M. Investigation of laminar convective heat transfer of a novel TiO_2-Carbon nanotube hybrid water-based nanofluid. Exp Heat Transf. 2016;29:1–15.
[110] Assael MJ, Antoniadis KD, Wakeham WA, Zhang X. Potential application of nanofluids for heat transfer. Int J Heat Mass Transf. 2019;138:597–607.
[111] Wen D, Lin G, Vafaei S, Zhang K. Review of nanofluids for heat transfer applications. Particuology. 2009;7:141–50.
[112] Ghafar SLMA, Hussein MZ, Zakaria ZAB. Synthesis and characterization of cockle shell-based calcium carbonate aragonite polymorph nanoparticles with surface functionalization. J Nanopart. 2017;8196172:1–12.
[113] Barki E, Ibrahim JS, Kuhe A, Iortyer HA. Experimental investigation of electrical conductivity and Ph of mango bark based nanofluid. Am J Eng Res. 2017;6(2):103–8.
[114] Raei B, Peyghambarzadeh SM, Asl RS. Experimental investigation on heat transfer and flow resistance of drag-reduction alumina nanofluid in a fin-and-tube heat exchanger. Appl Therm Eng. 2018;144:926–36.
[115] Varnaseri M, Peyghambarzadeh SM, Amiri M. Experimental study on optimum concentration of polyacrylamide for drag reduction and heat transfer performance in a compact heat exchanger. Heat Mass Transf. 2018;55(5):1503–11.
[116] Sadra P, Ramazani SAA. Investigation of the combination of TiO_2 nanoparticles and drag reducer polymer effects on the heat transfer and drag characteristics of nanofluids. Can J Chem Eng. 2017;96:6.
[117] Xu Y, Xiang X, Zheng G, Zeng X, Li Z, Ren T. Tribological performance of highly dispersed graphene oxide derivatives in vegetable oil. Tribol Int. 2018;126:39–48.
[118] Martin-Alfonso JE, Beltran FL, Valencia C, Franco JM. Effect of an alkali treatment on the development of cellulose pulp-based gel-like dispersions in vegetable oil for use as lubricants. Tribol Int. 2018;123:329–36.
[119] Gong K, Wu X, Zhao G, Wang X. Tribological properties of polymeric aryl phosphates grafted onto multi-walled carbon nanotubes as high-performances lubricant additive. Tribol Int. 2017;116:172–9.
[120] Esfe MH, Arani AAA, Rezaie M, Yan WM, Karimipour A. Experimental determination of thermal conductivity and dynamic viscosity of Ag-MgO/water hybrid nanofluid. Int Commun Heat Mass Transf. 2015;66:189–95.
[121] Xu G, Fu J, Dong B, Quan Y, Song G. A novel method to measure thermal conductivity of nanofluids. Int J Heat Mass Transf. 2019;130:978–88.
[122] Ahmadi MH, Mirlohi A, Nazari MA, Ghasempour R. A review of thermal conductivity of various nanofluids. J Mol Liq. 2018;265:181–8.
[123] Tlili I, Alkanhal TA, Barzinjy AA, Dara RN, Shafee A, Li Z. Investigation of thermal characteristics of carbon nanotubes: measurement and dependence. J Mol Liq. 2019;294:111564.
[124] Ebrahimi S, Saghravani SF. Influence of magnetic field on the thermal conductivity of the water based mixed Fe_3O_4/CuO nanofluid. J Magn Magn Mater. 2017;441:366–73.
[125] Keblinski P, Phillpot SR, Choi SUS, Eastman JA. Mechanisms of heat flow in suspensions of nano-size particles (nanofluids). Int J Heat Mass Transf. 2002;45:855–63.
[126] Aybar HA, Sharifpur M, Azizian MR, Mehrabi M, Meyer JP. A review of thermal conductivity models for nanofluids. Heat Transf Eng. 2015;36(13):1085–110.
[127] Eapen J, Rusconi R, Piazza R, Yip S. The classical nature of thermal conduction in nanofluids. J Heat Transf. 2010;132:102402–14.
[128] Fedele L, Colla L, Bobbo S. Viscosity and thermal conductivity measurements of water-based nanofluids containing titanium oxide nanoparticles. Int J Refrig. 2012;35(5):1359–66.
[129] Cui W, Shen S, Yang J, Wu S. Rotation and migration of nanoparticles for heat transfer augmentation in nanofluids by molecular dynamics simulation. Case Stud Therm Eng. 2015;6:182–93.
[130] Xie H, Fujii M, Zhang X. Effect of interfacial nanolayer on the effective thermal conductivity of nanoparticle-fluid mixture. Int Commun Heat Mass Transf. 2005;48:2926–32.
[131] Milanese M, Iocobazzi F, Colangelo G, Risi AD. An investigation of layering phenomenon at the liquid–solid interface in Cu and CuO based nanofluids. Int Commun Heat Mass Transf. 2016;103:564–71.
[132] Feng Y, Yu B, Xu P, Zou M. The effective thermal conductivity of nanofluids based on the nanolayer and the aggregation of nanoparticles. J Phys D Appl Phys. 2007;40:3164–71.
[133] Khodayari A, Fasano M, Bigdeli MB, Mohammasnejad S, Chiavazzo E, Asinari P. Effect of interfacial thermal resistance and nanolayer on estimates of effective thermal conductivity of nanofluids. Case Stud Therm Eng. 2018;12:454–61.
[134] Zhu H, Zhang C. Effects of nanoparticle clustering and alignment on thermal conductivities of Fe_3O_4 aqueous nanofluids. Appl Phys Lett. 2006;89:23123.
[135] Sarkar S, Selvam RP. Molecular dynamics simulation of effective thermal conductivity and study of enhanced thermal transport mechanism in nanofluids. J Appl Phys. 2007;102:74302–7.
[136] Topal I, Servantie J. Molecular dynamics study of thermal conductivity in nanofluids. Chem Phys. 2019;516:147–51.
[137] Avsec J. The combined analysis of phonon and electron heat transfer mechanism on thermal conductivity for nanofluids. Int Commun Heat Mass Transf. 2008;51:4589–98.
[138] Iacobazzi F, Milanese M, Colangelo G, Lomascolo M, Risi AD. An explanation of the Al_2O_3 nanofluid thermal conductivity based on the phonon theory of liquid. Energy. 2016;116:786–94.
[139] Sarviya RM, Fuskele V. Review on thermal conductivity of nanofluids. Mater Today: Proc. 2017;4:4022–31.
[140] Yang L, Xu J, Du K, Zhang X. Recent developments on viscosity and thermal conductivity of nanofluids. Powder Technol. 2017;317:348–69.
[141] Yildiz C, Arici M, Karabay H. Comparison of a theoretical and experimental thermal conductivity model on the heat transfer

performance of Al_2O_3–SiO_2/water hybrid-nanofluid. Int Commun Heat Mass Transf. 2019;140:598–605.
[142] Alawi OA, Sidik NAC, Xian HW, Kean TH, Kazi SN. Thermal conductivity and viscosity models of metallic oxides nanofluids. Int Commun Heat Mass Transf. 2018;116:1314–25.
[143] Commerce USS. National Institute of standards and technology. Thermophysical Prop fluid Syst [Internet]. 2018. Available from https://webbook.nist.gov/chemistry/fluid/.
[144] ASHRAE. Handbook – Fundamental (SI Edition). Atlanta, GA: American Society of Hearing, Refrigerating and Air-Conditioning Engineers Inc; 2009.
[145] Ranjbarzadeh R, Moradikazerouni A, Bakhtiari R, Asadi A, Afrand M. An experimental study on stability and thermal conductivity of water/silica nanofluid: eco-friendly production of nanoparticles. J Clean Prod. 2019;206:1089–100.
[146] Cabaleiro D, Nimo J, Pastoriza-Gallego MJ, Pineiro MM, Legido JL, Lugo L. Thermal conductivity of dry anatase and rutile nano-powders and ethylene and propylene glycol-based TiO_2 nanofluids. Heat Transf Eng. 2015;83:67–76.
[147] Moosavi M, Goharshadi EK, Youssefi A. Fabrication, characterization and measurement of some physicochemical properties of ZnO nanofluids. Int J Heat Fluid Flow. 2010;31:599–605.
[148] Akilu S, Baheta AT, Kadirgama K, Padmanabhan E, Sharma KV. Viscosity, electrical and thermal conductivity of ethylene and propylene glycol-based B-SiC nanofluids. J Mol Liq. 2019;284:780–92.
[149] Sonawane SS, Khedkar RS, Wasewar KL. Effect of sonication time on enhancement of effective thermal conductivity of nano TiO_2-water, ethylene glycol, and paraffin oil nanofluids and models comparisons. J Exp Nanosci. 2015;10(4):310–22.
[150] Codreanu C, Gavrila R, Morjan I. Experimental study concerning the influence of the base fluid properties on the thermal conductivity of nanofluids. 2007 International Semiconductor Conference. Vol. 1. IEEE; 2007.
[151] Sundar LS, Ramana EV, Singh MK, Sousa ACM. Thermal conductivity and viscosity of stabilized ethylene glycol and water mixture Al_2O_3 nanofluids for heat transfer applications: an experimental study. Int Commun Heat Mass Transf. 2014;56:86–95.
[152] Vajjha RS, Das DK, Kulkarni CP. Development of new correlations for convection heat transfer and friction factor in turbulent regime for nanofluids. Int J Heat Mass Transf. 2010;53:4607–18.
[153] Timofeeva EV, Yu W, France DM, Singh D, Routbort JL. Base fluid and temperature effects on the heat transfer characteristics of SiC in ethylene glycol/H_2O and H_2O nanofluids. J Appl Phys. 2011;109:14914–5.
[154] Xie H, Li Y, Yu W. Intriguingly high convective heat transfer enhancement of nanofluid coolants in laminar flows. Phys Lett A. 2010;2010:2566–8.
[155] Al-Waeli AHA, Chaichan MT, Sopian K, Kazem HA. Influence of the base fluid on the thermo-physical properties of PV/T nanofluids with surfactant. Case Stud Therm Eng. 2019;13(100340):1–8.
[156] Jana S, Salehi-Khojin A, Zhong WH. Enhancement of fluid thermal conductivity by the addition of single and hybrid nano-additives. Thermochim Acta. 2007;462:45–55.
[157] Jha N, Ramaprabhu S. Synthesis and thermal conductivity of copper nanoparticle decorated multiwalled carbon nanotubes based nanofluids. J Phys Chem C. 2008;112:9315–9.
[158] Yarmand H, Gharehkhani S, Ahmadi G, Shirazi SFS, Mohtazer E, Baradaran S, et al. Graphene nanoplatelets-silver hybrid nanofluids for enhanced heat transfer. Energy Convers Manag. 2015;100:10.
[159] Yarmand H, Zulkifli NWBM, Gharehkhani S, Sharazi SFS, Alrashed AAAA, Ali MAB, et al. Convection heat transfer enhancement with graphene nanoplatelet/platinum hybrid nanofluid. Int Commun Heat Mass Transf. 2017;88:120–5.
[160] Amiri A, Shanbedi M, Eshghi H, Heris SZ, Baniadam M. Highly dispersed multiwalled carbon nanotubes decorated with Ag nanoparticles in water and experimental investigation of the thermophysical properties. J Phys Chem C. 2012;116:7.
[161] Kim SH, Choi SR, Kim D. Thermal conductivity of metal-oxide nanofluids: particle size dependence and effect of laser irradiation. J Heat Transf. 2007;129:10.
[162] Madhesh D, Parameshwaran R, Kalaiselvam S. Experimental investigation on convective heat transfer and rheological characteristics of Cu-TiO_2 hybrid nanofluids. Exp Therm Fluid Sci. 2014;52:104–15.
[163] Ramachandran K, Hussein AM, Kadirgama K, Ramasamy D, Azmi WH, Tarlochan F, et al. Thermophysical properties measurement of nano cellulose in ethylene glycol/water. Appl Therm Eng. 2017;123:1158–65.
[164] Liu MS, Lin MCC, Huang IT, Wang CC. Enhancement of thermal conductivity with CuO for nanofluids. Chem Eng Technol. 2006;29(1):72–7.
[165] Choi SUS, Yu W, Hull JR, Zhang ZG, Lockwood FE. Nanofluids for vehicle thermal management. Vehicle Thermal Management Systems Conference & Exhibition. Vol. 1; 2001. p. 8.
[166] Eastman JA, Choi SUS, Li S, Yu W, Thompson LJ. Anomalously increased effective thermal conductivities of ethylene glycol-based nanofluids containing copper nanoparticles. Appl Phys Lett. 2001;78(6):718–20.
[167] Mostafizul RM, Bhuiyan MHU, Saidur R, Aziz ARA. Thermal conductivity variation for methanol based nanofluid. Int J Heat Mass Transf. 2014;76:350–6.
[168] Bohne D, Fischer S, Obermeier E. Thermal, conductivity, density, viscosity, and Prandtl-Number of ethylene glycol-water mixtures. Berichte Der Bunsenges Fur Phys Chem. 1984;88(8):739–42.
[169] Mintsa HA, Roy G, Nguyen CT, Doucet D. New temperature dependent thermal conductivity data for water-based nanofluids. Int J Therm Sci. 2009;48:363–71.
[170] Beck MP. Thermal conductivity of metal oxide nanofluids [dissertation]. USA: Georgia Institute of Technology; 2008.
[171] Suresh S, Venkitaraj KP, Selvakumar P, Chandrasekar M. Synthesis of Al_2O_3-Cu/water hybrid nanofluids using two step method and its thermal physical properties. Colloids Surf, A Physicochem Eng Asp. 2011;388:41–8.
[172] Hussein AM, Sharma KV, Bakar RA, Kadirgama K. A review of forced convection heat transfer enhancement and hydrodynamic characteristic of a nanofluid. Renew Sustain Energy Rev. 2014;29:734–43.

[173] Sudeep PM, Taha-Tijerina J, Ajayan PM, Narayanan TN, Anantharaman MR. Nanofluids based on fluorinated graphene oxide for efficient thermal management. RSC Adv. 2014;4(47):24887–92.
[174] Sundar LS, Singh MK, Sousa ACM. Enhanced heat transfer and friction factor of MWCNT-Fe_3O_4/water hybrid nanofluids. Int Commun Heat Mass Transf. 2014;52:11.
[175] Sedaghat F, Yousefi F. Synthesizes, characterization, measurements and modelling thermal conductivity and viscosity of graphene quantum dots nanofluids. J Mol Liq. 2019;2019(278):99–308.
[176] Batmunkh M, Tanshen MR, Nine MJ, Myekhlai M, Choi H, Chung H, et al. Thermal Conductivity of TiO_2 nanoparticles based aqueous nanofluids with an addition of a modified silver particle. Ind Eng Chem Res. 2014;53:8445–51.
[177] Omrani AN, Esmaeilzadeh E, Jafari M, Behzadmehr A. Effects of multi walled carbon nanotubes shape and size on thermal conductivity and viscosity of nanofluids. Diam Relat Mater. 2019;93:96–104.
[178] Kalantari A, Abbasi M, Hashim AM. Enhancement of thermal conductivity of size controlled silver nanofluid. Mater Today: Proc. 2019;7:612–8.
[179] Essajai R, Mzerd A, Hassnain N, Qjani M. Thermal conductivity enhancement of nanofluids composed of rod-shaped gold nanoparticles: Insights from molecular dynamics. J Mol Liq. 2019;293:1–8.
[180] Garg P, Alvarado JL, Marsh C, Carlson TA, Kessler DA, Annamalai K. An experimental study on the effect of ultrasonication on viscosity and heat transfer performance of multi-wall carbon nanotube-based aqueous nanofluids. Int Commun Heat Mass Transf. 2009;52:5090–101.
[181] Hamze S, Cabaleiro D, Estellé P. Graphene-based nanofluids: a comprehensive review about rheological behaviour and dynamic viscosity. J Mol Liq. 2021;325(115207):1–30.
[182] Yiamsawas T, Mahian O, Dalkilic AS, Kaewnai S, Wongwises S. Experimental studies on the viscosity of TiO_2 and Al_2O_3 nanoparticles suspended in a mixture of ethylene glycol and water for high temperature applications. Appl Energy. 2013;111:40–5.
[183] Watanabe. Drag reduction of complex mixtures. San Diego, United States: Elsevier Science Publishing Co Inc; 2018.
[184] Yu W, Xie H, Chen L, Li Y. Investigation of thermal conductivity and viscosity of ethylene glycol based ZnO nanofluid. Thermochim Acta. 2009;491:92–6.
[185] Aberoumand S, Jafarimoghaddam A, Moravej M, Aberoumand H, Javaherdeh K. Experimental study on the rheological behaviour of silver – heat transfer oil nanofluid and suggesting two empirical based correlations for thermal conductivity and viscosity of oil based nanofluids. Appl Therm Eng. 2016;101:1–33.
[186] Nguyen CT, Roy G, Gauthier C, Galanis N. Heat transfer enhancement using Al_2O_3-water nanofluid for an electronic liquid cooling system. Appl Therm Eng. 2006;27:6.
[187] Kallamu UM, Ibrahim JS, Sharifpur M, Meyer JP. Experimental investigation on viscosity of nanofluids prepared from banana fibre nanoparticles. The proceeding of 12th International Conference on Heat Transfer, Fluid Mechanics and Thermodynamics; Costa de Sol. Spain: 2016. p. 1713–8.
[188] Yanuar MS, Wibowo G, Gunawan. The flow characteristic of mud slurries and nata de coco fiber suspension in spiral pipe. The 10th International Meeting of Advance in Thermofluids (IMAT 2018); 2019. Vol. 2062. p. 20042–7.
[189] Zhang T, Zhang Y, Wang X, Liu S, Yao Y. Characterization of the nano-cellulose aerogel from mixing CNF and CNC with different ratio. Mater Lett. 2018;229(4):103–6.
[190] Singh N, Chand G, Kanagaraj S. Investigation of thermal conductivity and viscosity of carbon nanotubes-ethylene glycol nanofluids. Heat Transf Eng. 2012;33(9):821–7.
[191] Lee PFW, Duffy GG. Relationships between velocity profiles and drag reduction in turbulent fiber suspension flow. AIChE J. 1976;22(4):4.
[192] Kwek D, Crivoi A, Duan F. Effects of temperature and particle size on thermal properties measurements of Al_2O_3-water nanofluids. J Chem Eng Data. 2010;55:5690–5.
[193] Adio SA, Sharifpur M, Meyer JP. Influence of ultrasonication energy on the dispersion consistency of Al_2O_3-glycerol nanofluid based on viscosity data, and model development for the required ultrasonication energy density. J Exp Nanosci. 2015;11(8):630–49.
[194] Minakov AV, Rudyak VY, Pryazhnikov MI. Rheological behaviour of water and ethylene glycol based nanofluids containing oxide nanoparticles. Colloids Surf, A Physicochem Eng Asp. 2018;554:279–85.
[195] Talari VK, Thamida SK, Sastry RC. Determination of optimum concentration of nanofluid for process intensification of heat transfer using corrugated plate type heat exchanger. Chem Prod Process Model. 2018;14(20080002):1–15.
[196] Rejvani M, Alipour A, Vahedi SM, Chamkha AJ, Wongwises S. Optimal characteristics and heat transfer efficiency of SiO_2/water nanofluid for application of energy devices: a comprehensive study. Int J Energy Res. 2019;43(14):8548–71.
[197] Esfe MH, Hajmohammad MH, Sina N, Afrand M. Optimization of thermophysical properties of Al_2O_3/water-EG (80:20) nanofluids by NSGA-II. Phys E Low Dimens Syst Nanostruct. 2018;103:264–72.
[198] Cabaleiro D, Estellé P, Navas H, Desforges A, Vigolo B. Dynamic viscosity and surface tension of stable graphene oxide and reduced graphene oxide aqueous nanofluids. J Nanofluids. 2018;7(6):1081–88.
[199] Perry RH. Perry's chemical engineers' handbook. 7th edn. University of Kansas: McGraw-Hill; 1997.
[200] Mishra P, Chakraverty A, Banerjee HD. Studies on physical and thermal properties of rise husk related to its industrial application. J Mater Sci. 1986;21:4.
[201] Alavez-Ramirez R, Chinas-Castillo F, Morales-Dominguez VJ, Ortiz-Guzman M. Thermal conductivity of coconut fibre filled ferrocement sandwich panels. Constr Build Mater. 2012;37:7.
[202] Sorayot C, Julie MT, Julia AK, Gregory MO. Thermal conductivity of graphene nanoplatelet/cycloaliphatic epoxy composites: multiscale modelling. Carbon. 2018;140:653–63.
[203] Kim P, Shi L, Majumdar A, McEuen PL. Thermal transport measurement of individual multiwalled nanotubes. Phys Rev Lett. 2001;87(21):4.
[204] Yang DJ, Zhang Q, Chen G, Yoon SF, Ahn SG, Ahn J, et al. Thermal conductivity of multiwalled carbon nanotubes. Phys Rev B. 2002;66(165440):6.
[205] Touloukian YS, Saxena SC, Hestermans P. Thermophysical properties of matter. TPRC Data Ser. 1970;11:804.
[206] Cengel YA, Cimbala JM, Turner RH. Fundamental of thermal-fluid sciences. 4th edn. New York: McGraw Hill; 2012.

[207] Madhesh D, Kalaiselvam S. Experimental analysis of hybrid nanofluid as a coolant. Proc Eng. 2014;97:1667–75.
[208] Yarmand H, Gharehkhani S, Shirazi SFS, Goodarzi M, Amiri A, Sarsam WS, et al. Study of synthesis, stability and thermophysical properties of graphene nanoplatelet/platinum hybrid nanofluid. Int Commun Heat Mass Transf. 2016;77:15–21.
[209] Moldoveanu GM, Huminic G, Minea AA, Huminic A. Experimental study on thermal conductivity of stabilized Al_2O_3 and SiO_2 nanofluids and their hybrid. Int Commun Heat Mass Transf. 2018;127:450–57.
[210] Kumar MS, Vasu V, Gopal AV. Thermal conductivity of rheological studies for Cu-Zn hybrid nanofluids with various basefluids. J Taiwan Inst Chem Eng. 2016;66:321–27.
[211] Devarajan M, Krishnamarthy NP, Balasubramanian M, Ramani B, Wongwises S, El-Naby KA, et al. Thermophysical properties of CNT and CNT/Al_2O_3 hybrid nanofluid. Micro Nano Lett. 2018;13:617–21.
[212] Kim D, Kwon Y, Cho Y, Li C, Cheong S, Hwang Y, et al. Convective heat transfer characteristics of nanofluids under laminar and turbulent flow conditions. Curr Appl Phys. 2009;9:e119–23.